BRNO UNIVERSITY OF TECHNOLOGY
VYSOKÉ UČENÍ TECHNICKÉ V BRNĚ

FACULTY OF MECHANICAL ENGINEERING
FAKULTA STROJNÍHO INŽENÝRSTVÍ

INSTITUTE OF PHYSICAL ENGINEERING
ÚSTAV FYZIKÁLNÍHO INŽENÝRSTVÍ

EFFECT OF ION BEAM IRRADIATION AND ANNEALING ON MAGNETIC PROPERTIES OF FERH NANOSTRUCTURES
VLIV OZAŘOVÁNÍ IONTOVÝM SVAZKEM A ŽÍHÁNÍ NA MAGNETICKÉ VLASTNOSTI FERH NANOSTRUKTUR

BACHELOR'S THESIS
BAKALÁŘSKÁ PRÁCE

AUTHOR — Oleksii Zadorozhnii
AUTOR PRÁCE

SUPERVISOR — Dr. Ing. Michal Staňo
VEDOUCÍ PRÁCE

BRNO 2019

VYSOKÉ UČENÍ TECHNICKÉ V BRNĚ
FAKULTA STROJNÍHO INŽENÝRSTVÍ

Zadání bakalářské práce

Ústav:	Ústav fyzikálního inženýrství
Student:	**Oleksii Zadorozhnii**
Studijní program:	Strojírenství
Studijní obor:	Základy strojního inženýrství
Vedoucí práce:	**Dr. Ing. Michal Staňo**
Akademický rok:	2018/19

Ředitel ústavu Vám v souladu se zákonem č.111/1998 o vysokých školách a se Studijním a zkušebním řádem VUT v Brně určuje následující téma bakalářské práce:

Vliv ozařování iontovým svazkem a žíhání na magnetické vlastnosti FeRh nanostruktur

Stručná charakteristika problematiky úkolu:

Strukturní, magnetické a další vlastnosti materiálů mohou být lokálně změněny např. pomocí ozařování fokusovaným iontovým svazkem. V případě slitiny FeRh s B2 (CsCl) strukturou může ozařování vést ke změně teploty fázové přeměny z antiferomagnetické (nízkoteplotní) na feromagnetickou (vysokoteplotní) fázi. Příliš vysoká dávka iontů však může zcela potlačit tuto přeměnu. Jelikož se fokusovaný iontový svazek používá také k výrobě nanostruktur z tenkých vrstev, je důležité vědět o vlivu svazku na materiál a také jak můžeme obnovit metamagnetickou přeměnu v (částečně) ozářených strukturách, např. pomocí žíhání.

Cíle bakalářské práce:

1) Proveďte rešerši na téma vlivu ozařování pevných látek svazkem urychlených iontů s důrazem na ovlivnění magnetických a strukturních vlastností tenkých vrstev a nanostruktur ze slitiny FeRh.
2) Modifikujte lokálně tenké vrstvy FeRh pomocí fokusovaného iontového svazku (použijte různé dávky iontů a případně i energie).
3) Pomocí magnetických mikroskopií (např. mikroskopie magnetických sil) za různých teplot porovnejte magnetické vlastnosti (přítomnost magnetických domén) pro různé dávky iontů a také vliv žíhání.

Seznam doporučené literatury:

AIKOH, K., KOSUGI,S., MATSUI, T. and IWASE, A., Quantitative control of magnetic ordering in FeRh thin films using 30 keV Ga ion irradiation from a focused ion beam system. Journal of Applied Physics. 2011, 109(7), 07E311. DOI: 10.1063/1.3549440.

TOHKI, A., AIKOH, K., IWASE, A., et al. Effect of high temperature annealing on ion-irradiation induced magnetization in FeRh thin films. Journal of Applied Physics. 2012, 111(7), 07A742. DOI: 10.1063/1.3687133.

KITTEL, Ch. Introduction to solid state physics. 8th ed. New York: John Wiley, 2005, ISBN 0-47--68057-5.

FREY, H. and KHAN, R. H. ed. Handbook of thin-film technology. Heidelberg: Springer, 2015, ISBN 978-3-642-05429-7.

Termín odevzdání bakalářské práce je stanoven časovým plánem akademického roku 2018/19

V Brně, dne

L. S.

prof. RNDr. Tomáš Šikola, CSc. ředitel ústavu

doc. Ing. Jaroslav Katolický, Ph.D. děkan fakulty

Abstract

The first order phase transition from antiferromagnetic to ferromagnetic state in $Fe_{50}Rh_{50}$ at 370 K makes it a suitable material for next generation spin electronic devices with a low power consumption.

This work deals with the ways how the phase transition temperature of iron-rhodium (FeRh) can be tuned locally in thin films, using focused ion beam (FIB) and thermal annealing. FIB irradiation approach was chosen due to the fact that FeRh displays magnetic sensitivity to the degree of its chemical ordering. Thermal annealing enables the relaxation of the structure and restoration of its crystallinity. The magnetic patterns were manufactured using gallium-based FIB and annealed under ultra high vacuum. The topography as well as magnetic behaviour of these ion irradiated patterns were investigated using atomic and magnetic force microscopies at different temperatures, showing a clear dependence between ion irradiation dose and the magnetic response in pre- and post-annealed states.

Keywords

FeRh, iron-rhodium alloy, thin film, ion irradiation, annealing, focused ion beam, magnetic force microscopy, phase transition

Abstrakt

Fázový přechod prvního řádu z antiferomagnetického do feromagnetického stavu v $Fe_{50}Rh_{50}$ z něj činí vhodný materiál pro novou generaci spintronických zařízení s nízkou spotřebou.

Tato práce se zabývá způsoby, jak lze teplotu fázového přechodu železo-rhodia (FeRh) lokálně ovlivnit pomocí fokusovaného iontového svazku (FIB) a žíhání. FIB byl zvolen vzhledem k tomu, že slitina FeRh vykazuje magnetickou citlivost na stupeň jejího chemického uspořádání. Tepelné žíhaní umožňuje obnovení krystalografického uspořádání, a uvolnění mřížkových defektů a dislokací. Magnetické vzory byly vyrobeny za použití FIB na bázi galia a žíhány ve vakuu. Topografie a magnetické chování těchto iontově ozářených vzorů byly zkoumány pomocí mikroskopie atomárních a magnetických sil při různých teplotách, a ukázaly jasnou závislost mezi dávkou iontového záření a magnetickou odezvou ve stavu před a po žíhání.

Klíčová slova

FeRh, slitina železo-rhodia, tenká vrstva, ozařování ionty, fokusovaný iontový svazek, mikroskopie magnetických sil, fázová přeměna.

I declare that I worked on my bachelor's thesis on the topic of *Effect of ion beam irradiation and annealing on magnetic properties of FeRh nanostructures* under the guidance of the supervisor, Dr. Ing. Michal Staňo, using the literature listed in the Bibliography section.

Zadorožnij Oleksii

Acknolwedgements:

First and foremost, I would like to extend my deepest gratitude to my supervisor, Dr. Ing. Michal Staňo for limitless patience and support provided, as well as continuous support and understanding throughout this work. I would also like to thank Bc. Lucie Motyčková under the supervision of M.Sc. Jon Ander Arregi Uribeetxebarria for providing the FeRh sample, and the whole FeRh team under the leadership of Ing. Vojtěch Uhlíř Ph.D for moral support, insights and friendly atmosphere.

This work was carried out with the support of CEITEC Nano Research Infrastructure (ID LM2015041, MEYS CR, 2016–2019), CEITEC Brno University of Technology.

Table of Contents

Introduction

$Fe_{50}Rh_{50}$, both bulk and thin film samples have been an object of great interest in the recent years, specifically due to the first order, anti-ferromagnetic to ferromagnetic phase transition which takes place close to room temperature (370 K) [1]. FeRh has a potential to be used in temperature and magnetic field-dependent sensors, and also as the recording media material for magnetic recording technology (Heat-Assisted Magnetic Recording) [2].

In $Fe_{50}Rh_{50}$ thin film, phase transition takes place close to 370 K [1]. During the first-order phase transition, a symmetric hysteresis loop occurs, as a result of difference in energetic preferences for antiferromagnetic and ferromagnetic phases' existence (Figure 2.1); both phases can coexist during the transitiion [3]. This phase transition is also accompanied by a change in the electronic structure, during which the resistivity drops sharply (Figure 2.1). FeRh is also set among other binary alloys of ferromagnetic and paramagnetic metals which are magnetically sensitive to the degree of their chemical order. Examples include FeAl and FeV which show similar dependency to FeRh of their magnetism on the degree of their chemical ordering [4,5]. As the degree of chemical disorder increases, the $Fe_{50}Rh_{50}$ alloy exhibits increasingly ferromagnetic behaviour at room temperature, and remains meta-stable. As we increase the disorder even further, the alloy loses its ferromagnetic properties and behaves paramagnetically.

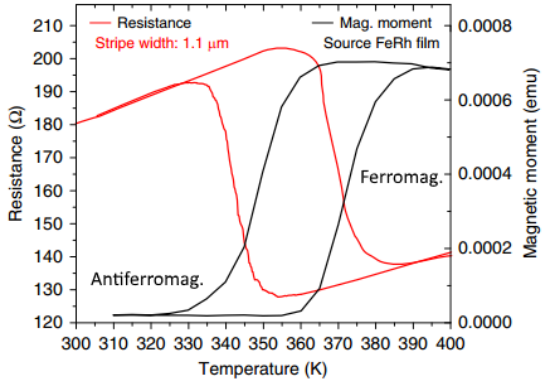

Figure 2.1: FeRh thin film phase transition probed by magnetometry and electrical resistance (transport) measurements. Taken from [15].

This work investigates the effects of ion irradiation and thermal annealing of FeRh thin films, as well as experimental evaluation of locally ion irradiated and thermally annealed patterns. The literature review included within this work covers the state-of-the-art for FeRh thin film ion irradiation and thermal annealing. The experimental part is focused on verifying the behaviour of FeRh thin film for locally ion-irradiated and globally annealed FeRh thin film. The magnetic behaviour was investigated using magnetic force microscopy at different temperatures.

Section 3 focuses on the introduction to magnetism in solid matter, followed by the more in-depth look at the properties of $Fe_{50}Rh_{50}$ thin films, which also includes the information obtained from the literature search. Section 4 describes the instruments and methods used, as well as experiments devised. In Section 5, the results are provided and discussed.

2 Introduction to magnetism

This section covers basic quantities in magnetism – magnetic moment and magnetization. Moreover, it also describes classes of materials according to their magnetic ordering in an external magnetic field. These include: paramagnetic, diamagnetic, ferromagnetic and anti-ferromagnetic materials. Greatly expanded and complete description can be found in the textbooks (Blundell, 2001; Kittel, 2005).

2.1 Magnetic moments

In classical mechanics, a magnetic moment is defined as a current flowing around infinitesimal loop (Figure 3.1).The magnetic moment $d\mu$ is then defined as:

$$d\vec{\mu} = I\, d\vec{S} \tag{3.1}$$

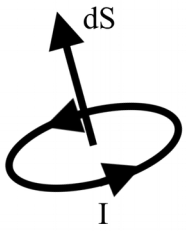

Figure 3.1: Magnetic moment

where I is current in Amperes, and **dS** is an element of the surface, with its vector normal to the loop (Figure 2.1). The magnetic moment is measured in A.m^2.

This object is also equivalent to a magnetic dipole, and it can be described as an object consisting of two magnetic monopoles of opposite "charge" separated by a small distance in the same direction as vector **dS** [6]**.**

Motion of the electron around the atom is also the cause of angular momentum, meaning that there is a direct association of non-zero mass charge motion with both magnetic moment and angular momentum. Magnetic moment $\vec{\mu}$ lies in the same axis as the angular momentum $\vec{L}$ of the electron, and is proportional to it [6]. It can be written down as:

$$\vec{\mu} = \gamma \vec{L} \tag{3.2}$$

where ɣ is known as gyromagnetic ratio.

As a consequence of the angular momentum and magnetic moment relationship, atom with an orbiting electron in an external magnetic field will precess, as the magnetic moment vector attempts to orient itself towards the direction of the external magnetic field in order to reduce its magnetic potential energy, given by the following equation:

$$E = -\vec{\mu} \cdot \vec{B} \tag{3.3}$$

In order for the vectors of both magnetic moment and external magnetic field to face the same direction, torque moment $\vec{G}$ is generated:

$$\vec{G} = \vec{\mu} \times \vec{B} \tag{3.4}$$

For the case of a massless charge, the magnetic moment is oriented in the same direction as magnetic field. In contrast, for a massive particle precession would occur. As the torque $\vec{G}$ is equal to the rate of change of angular momentum, Eq. 3.4 can be re-written as:

$$\frac{d}{dt}\vec{\mu}=\gamma\,\vec{\mu}\times\vec{B} \tag{3.5}$$

Which points out that change in magnetic moment is perpendicular to both the magnetic moment and external magnetic field $\vec{B}$, causing precession.

Another factor that plays a role in the overall magnetic moment of an atom is the electron's property called intrinsic magnetic moment, which is associated with an intrinsic angular momentum. This property is called spin, which is described by a spin quantum number s, which for an electron can have the values of $\pm(1/2)$ [6].

The angular momentum of an electron always takes half-integer or integer multiples of reduced Planck constant ($\hbar$ = 1.054 571 800×10^{-34} J.s). Angular momenta (orbital angular momentum and intrinsic angular momentum) can combine [6].

2.2 Magnetization

The magnetization $\vec{M}$ is defined as the magnetic moment per unit volume, and is an approximation of an environment in which the number of magnetic moments is large enough for us to approximate the sum of individual magnetic moments by a continuum. This makes $\vec{M}$ a vector field that is continuous throughout the solid, excluding the edges[6].

In free space, the magnetic field can be described by the vector fields $\vec{B}$ and $\vec{H}$, their relationship being:

$$\vec{B}=\mu_0\vec{H} \tag{3.6}$$

Where $\mu 0$ is a constant called permeability of free space ($\mu_0=1.25663706\cdot10^{-6}\,m\,kg\,s^{-2}\,A^{-2}$). The two magnetic fields $\vec{B}$ and $\vec{H}$ are related by a scaling factor, measured in Tesla and A/m respectively[6].

For the case of magnetic solids, the connection between $\vec{B}$ and $\vec{H}$ becomes more complicated, as the two fields can vary in both magnitude and direction. Generally, this relationship can be written as:

$$\vec{B}=\mu_0(\vec{H}+\vec{M}) \tag{3.7}$$

If the magnetization $\vec{M}$ is related to the field $\vec{H}$ linearly, as in the case of free space, the solid in which it occurs is called a linear material [6], and we can describe this relation as:

$$\vec{M}=\chi\vec{H} \tag{3.8}$$

In which χ is a dimensionless quantity called magnetic susceptibility.

In analogy to the Eq. 3.5, the relation describing the precession of the magnetization and the damping of it, is called the Landau-Lifshitz equation [6]:

$$\frac{d}{dt}\vec{M} = -\gamma\,\vec{M}\times\vec{H}_{eff} - \text{ж}\,\vec{M}\times(\vec{M}\times\vec{H}_{eff}) \tag{3.9}$$

where γ is the gyromagnetic ratio of an electron, and ж is a phenomenological damping parameter. $\vec{H}_{eff}$ is the effective field, combination of the external magnetic field and other contributions.

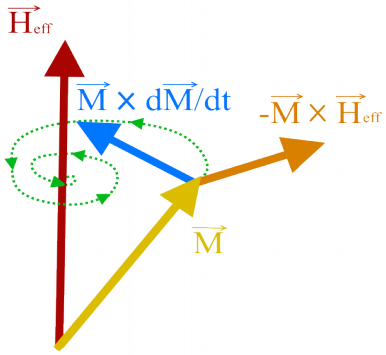

Figure 3.3: Visualized Landau-Lifshitz-Gilbert equation. Precession term (orange), damping term (blue), trajectory of the magnetization (green). Unlike Landau-Lifshitz equation, damping term is a function of time derivative of magnetization. Effective field is considered to be constant.

2.3 Diamagnetism

Diamagnetism is a weak and negative magnetic susceptibility, meaning that the external magnetic field induces a magnetization which is opposite to it, and it is present in all materials to some extent.

In Langevin's theory of diamagnetism, which is valid for non-conducting solids, it is explained that the interior of the material is shielded from the external field by outermost atoms, which in analogy to Lenz's law, have their orbital electrons precess to create a magnetic moment opposite to the external magnetic field [7].

In order to describe diamagnetism of solids with conducing electrons, Landau's theory of diamagnetism is used, which takes the conducting electrons into account [8].

2.4 Paramagnetism

Paramagnetism corresponds to a positive susceptibility to an external magnetic field, causing the magnetic moments to align in the same direction as the external magnetic field. Paramagnetism occurs in materials which have randomly oriented magnetic moments due to very weak magnetic interaction between the neighbouring atoms, the magnetic moments being effectively independent. The application of a magnetic field lines them up, the degree of this "lining up", and, hence, induced magnetization depends on the strength of the applied magnetic field [6].

In semi-classical treatment of paramagnetism the fact that magnetic moments can point only

along certain directions as an effect of quantization is ignored. Using this assumption Curie's law can be derived, which states that the magnetic susceptibility is inversely proportional to the temperature [6]:

$$\chi = \frac{C_{Curie}}{T} \tag{3.8}$$

Where χ is magnetic susceptibility, T is the absolute temperature, and C_{Curie} is the Curie constant.

2.5 Interactions

This section will cover the mechanisms which enable the existence of ferromagnetism and anti-ferromagnetism as such.

The first interaction that can be of interest is called magnetic dipolar interaction. Two magnetic dipoles $\vec{\mu}_1$ and $\vec{\mu}_2$ separated by distance $\vec{r}$ have a dipolar energy equal to:

$$E_d = \frac{\mu_0}{(4\pi r^3)}\left[\vec{\mu}_1 \cdot \vec{\mu}_2 - \frac{3}{r^2}(\vec{\mu}_1 \cdot \vec{r})(\vec{\mu}_2 \cdot \vec{r})\right] \tag{3.10}$$

It is governed by the degree of their separation and mutual alignment (Figure 3.4).

Exchange interaction is a mechanism that enables the long-range ferromagnetic and anti-ferromagnetic ordering. In its core, exchange interactions are electrostatic interactions of charges which are lead down the path of least resistance, to the local minimum of energy (Figure 3.5). As such, the charges find the position in which they are repulsing one another the least, by being positioned as far away from one another as possible [6].

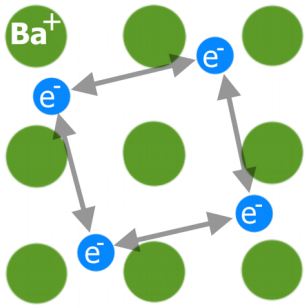

Figure 3.5: Exchange interaction

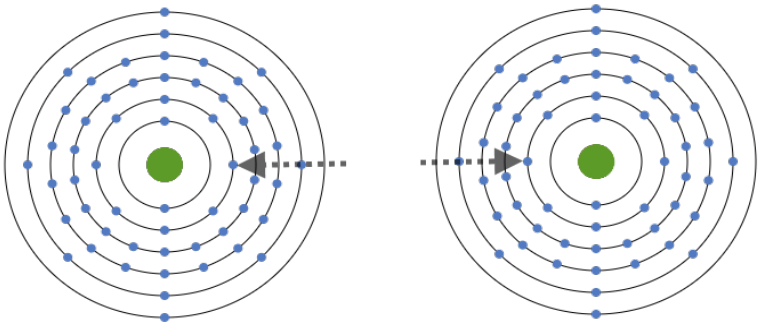

Figure 3.6: Direct exchange interaction

Direct exchange occurs when electrons of neighboring magnetic atoms interact with one another by the means of an exchange interaction (Figure 3.6). As the name suggests, the interaction happens without an intermediary. It is of limited magnitude due to the fact that the electron orbitals are located very close to the atomic nucleus, limiting the effectiveness of the direct exchange interactions as they are simply unlikely to happen [6].

Indirect exchange in metals can be mediated by the conduction electrons. A localized magnetic moment spin-polarizes the conduction electrons, and this polarization in turn couples to a neighboring localized magnetic moment a distance $\vec{r}$ away. It is called RKKY(Ruderman, Kittel, Kasuya and Yoshida) interaction [6].

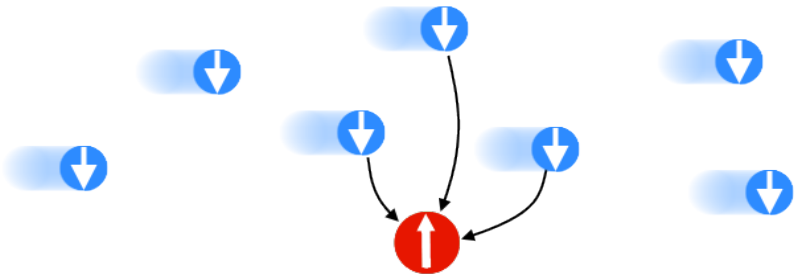

Figure 3.7: RKKY interaction. Conducting, spin-polarized electrons (blue) are magnetically coupled to the orbital electron (red).

Anisotropic exchange interaction, also known as spin-orbit interaction, can also play a role in magnetic properties of ferromagnets. The exchange takes place between the excited state of one ion, and the ground state of the other ion. This interaction is known as Dzyaloshinskii-Moriya interaction [6,9].

2.6 Ferromagnetism

Main property of a ferromagnet is its spontaneous magnetization in presence or in absence of an external magnetic field. All magnetic moments are locally arranged along a single unique direction, these local spots are called magnetic domains. This effect is caused by the exchange interactions [6,9]. For a ferromagnet in an external magnetic field **B**, the appropriate Hamiltonian to solve is:

$$\hat{H} = -\sum_{ij} \vec{J}_{ij} \vec{S}_i \cdot \vec{S}_j + g \mu_B \sum_{ij} \vec{S}_j \cdot \vec{B} \qquad (3.11)$$

which is also known as Heisenberg Hamiltonian. The first term on the right is called Heisenberg exchange energy, the second term on the right is called Zeeman energy.

where $\hat{H}$ is the Hamiltonian operator, which describes the total energy of the system (sum of potential and kinetic energies).

$\vec{J}_{ij}(r_{ij})$ is called the exchange integral, for *i*th and *j*th atoms, with $\vec{r}_{ij}$ denoting the radius vector joining the *i*th and *j*th lattice sites. Ferromagnetic behaviour is signified by the positive value of the exchange integral in Eq. (3.11).

$\vec{S}_i$ and $\vec{S}_j$ are are the atomic spins at *i*th and *j*th lattice positions
g is so-called g-factor, a dimensionless proportionality constant that describes the relation between magnetic moment of a particle and its angular momentum quantum number [6].

μ_B is the Bohr magneton, a physical constant and the natural unit used for the expression of magnetic moment of an electron caused by its orbital or spin angular momentum. (μ_B = 9.274.10^-24 J/T).

In order to make progress solving the eqn(10), the approximation has to be created, which results in a conception of the so-called Weiss molecular field. After the appropriate steps are taken [26], the Heisenberg Hamiltonian is reduced to:

$$\hat{H} = g\,\mu_B \sum_i \vec{S}_i \cdot (\vec{B} + \vec{B}_{mf}) \tag{3.12}$$

Which is equivalent to a paramagnet in an external magnetic field $\vec{B} + \vec{B}_{mf}$ The assumption underlining this approach is that all magnetic ions experience the same molecular field, which may not hold true at temperatures close to a magnetic phase transition [6].

Since the molecular field describes the effect of the ordering of the system, one can assume that:

$$\vec{B}_{mf} = \lambda \vec{M} \tag{3.13}$$

where λ is a constant that relates the molecular field and magnetization. For a ferromagnet, it is greater than zero. Due to large Coulomb energy (energy associated with electrostatic forces) involved during exchange interactions, the molecular field is often found to be large in ferromagnets [6,9].

At low temperatures, the moments are aligned by the molecular field, without any external field present. The alignment of these magnetic moments causes the internal molecular field which causes the alignment in the first place, creating a self-reinforcing loop [6,9].

At low temperatures, this magnetic ordering is self-sustaining. As the temperature is raised, this ordering is disturbed by thermal fluctuations, and at a critical temperature, called Curie temperature, this magnetic ordering will be destroyed (Figure 3.8). This phenomenon is described by the Weiss-Curie law:

$$\chi = \frac{C_{Curie}}{(T - T_C)} \tag{3.14}$$

C_{Curie} is the Curie constant, Tc is the Curie temperature, and T is the temperature of the solid.

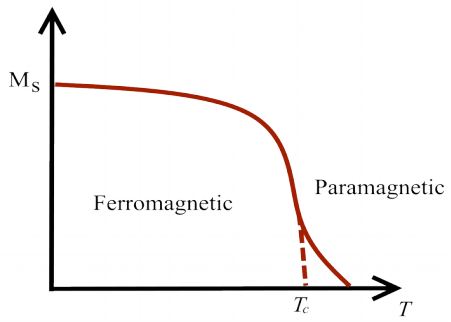

Figure 3.8: Saturated magnetization as a function of temperature of a ferromagnet. The saturated magnetization drops sharply at Curie temperature. Ferromagnetic ordering is lost.

2.6.1 Magnetic domains

Magnetic domains are areas of ferromagnetic material in which the magnetization has local orientation with respect to other domains (Figure 3.9). The formation of these domains saves energy. Due to the relationship between magnetization and the external magnetic field, the magnetic field starts to diverge at the edges of the sample, producing demagnetizing field, which costs energy to maintain [6,9].

Formation of the domains is a balancing act between the energy required for the formation of a domain wall, and the energy required for a demagnetizing field (Figure 3.10).

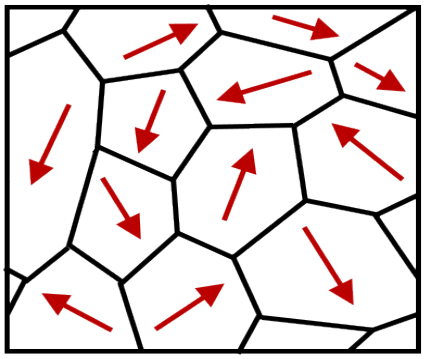

Figure 3.9: local ferromagnetic domains

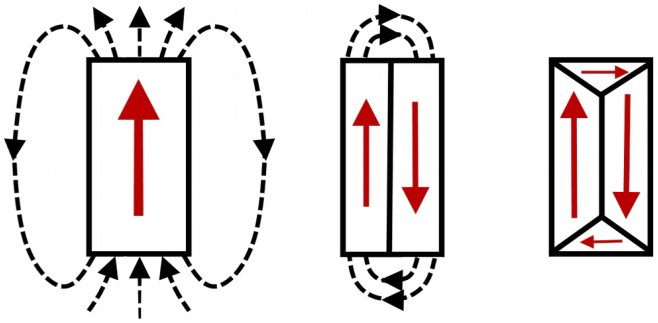

Figure 3.10: Formation of magnetic domains (Inspired by Blundell, 2001)

2.6.2 Magnetocrystalline anisotropy

In certain crystallographic directions, crystal magnetization is more preferable than in others. This leads to the separation of these axes into an easy axis and a hard axis [ ].

Easy axis is the one in which anisotropic energy reaches its minimum, with uniaxial anisotropic energy (simple particular case) being defined as:

$$E_a = K_u \sin^2(\theta) \tag{3.15}$$

where K_u is uniaxial anisotropy constant, and θ is the angle of deviation from the easy axis.

2.6.3 Magnetic hysteresis

Magnetic hysteresis occurs in ferromagnetic and anti-ferromagnetic materials as a functi n of external field H. After magnetic saturation of the ferromagnet by an applied field (Figure 3.11, curve o-a), reducing the external magnetic field to zero (Figure 3.11, curve a-b) return the ferromagnet to the state of remanent magnetization M_R. In order to change the direct on of the magnetization, a coercive field H_C is needed.. In order to demagnetize the sample, oscillating decaying external magnetic field must be applied [6].

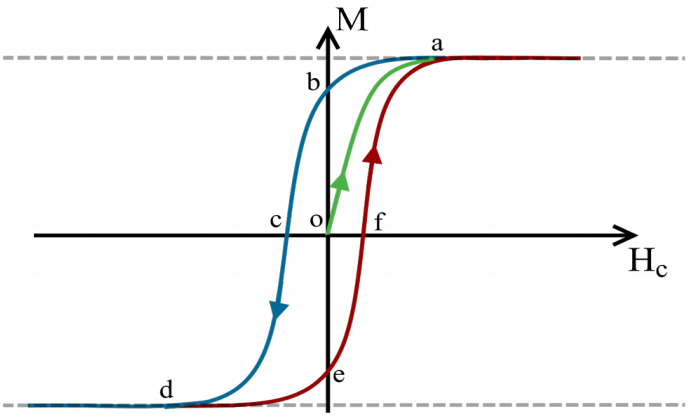

Figure 3.11: Magnetization as a function of external (coercive) magnetic field

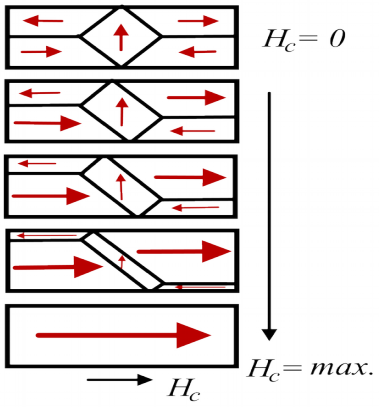

Figure 3.12: Magnetic domain growth as a function of external (coercive) magnetic field. (Adapted from [6])

One of the main processes that take place during this change of magnetization is domain-wall motion. Favourably-oriented domains tend to grow in size at the expense of other domains (Figure 3.12).

In a sufficiently high external magnetic field, domains can change their orientation to the one pointing in the direction of crystallographic easy axis closest to the field direction [6].

Within an even stronger magnetic field, the domains will be oriented in the direction of the magnetic field, irrespective of crystallographic easy axis [6].

2.7 Anti-Ferromagnetism

If the exchange integral for Eq. 3.11 is negative, the molecular field is oriented in such a manner that it is favourable for nearest magnetic moments to position themselves antiparallel to one another, thus causing antiferromagnetism.

This occurs frequently in systems which are said to have two interpenetrating sublattices (Figure 3.13), on one of which the magnetic moments point in one direction, and on the other in the opposite direction [6].

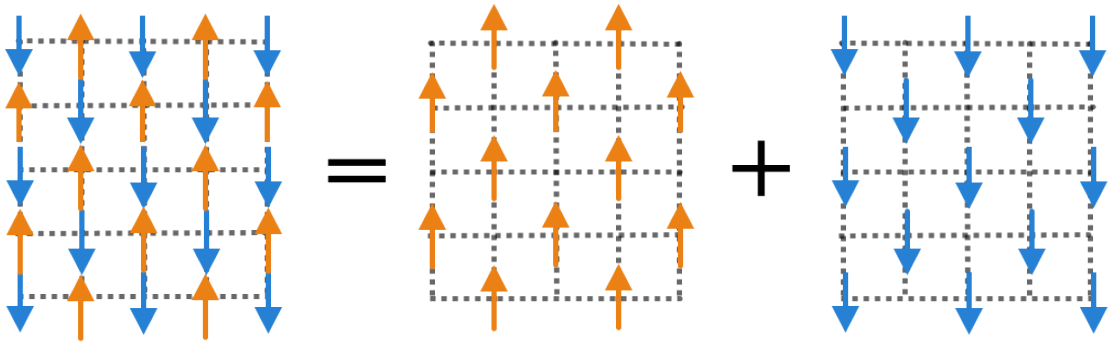

Figure 3.13: Antiferromagnet as two supersposed ferromagnetic sublattices.

In this case, if the symmetry is not broken by a strong external magnetic field, or introduced internal defects, the total (net) magnetization is zero.

Susceptibility of an anti-ferromagnet is described by the previously mentioned Weiss-Curie law (Equation 3.14), with the main difference being that the term -Tc describing curie temperature is replaced by +T_N describing Neel temperature (Figure 3.14) [32 ½].

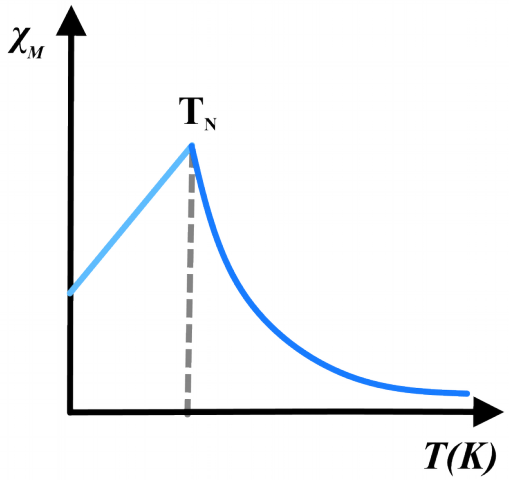

Figure 3.14: Dependence of magnetic susceptibility on the temperature for an antiferromagnet, where T_N denotes the Neél temperature.

2.7.1 Strong magnetic field effects

In the case of a strong enough magnetic field acting on an antiferromagnet, the internal molecular field will be overpowered, and the magnetic moments will be forced to align parallel to one another. As the external field is increased, the effects are similar to the ones discussed in the section dedicated to magnetic hysteresis, but the process strongly depends on the orientation of the applied field in relation to the initial sub-lattice magnetization direction [6].

For the case of applied field being perpendicular to sub-lattice magnetization directions, as the external field increases, the magnetic moments become increasingly deflected, until they are aligned with the external magnetic field [6].

In the scenario of parallel alignment, for weaker magnetic fields the sub-lattice's magnetic moments stay aligned in their original direction irrespective of varying external field. At a critical field intensity, the sub-lattice magnetization changes into a different configuration, this is known as spin-flop transition (Figure 3.15) [6].

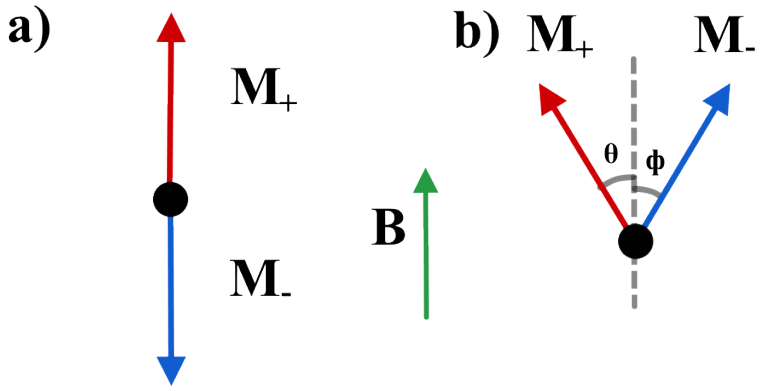

Figure 3.15: sub lattice magnetizationalignment. a) initial configuration b) spin-flopped configuration

The antiferromagnetic phase corresponds to $\theta = 0$, and $\phi = \pi$. (Figure 3.15, a) the spin-flop phase corresponds to $\theta = \phi$, the exact angle of this alignment is influenced by the exchange coupling, magnetic anisotropy, as well as crystallographic easy axis orientation [6].

For the antiferromagnet, the energy required for the maintenance of the antiferromagnetic arrangement can be described as:

$$E = -AM^2 - \Delta \tag{3.15}$$

Where A is a constant related to exchange coupling, M is magnetization magnitude, and Δ is the term accounting for the crystallographic easy axis [6].

Spin-flop occurs when spin-flop phase becomes less energy demanding than antiferromagnetic

phase (Figure 3.16).

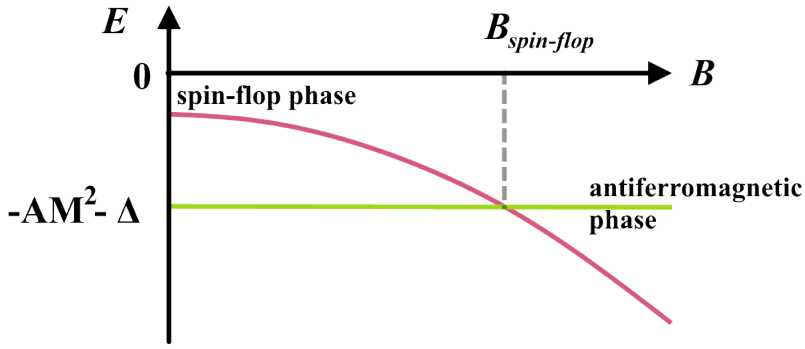

Figure 3.16: antiferromagnetic and spin-flop phase energy requirements as a function of external magnetic field

There is largely no effects of external field on anti-ferromagnet until this spin-flop transition takes place. After spin flop, the magnetization will keep on increasing up to the point of magnetic saturation.

However, in the case of anisotropy effect contribution (Δ) being significant, and the external field being aligned with the magnetization axis, no spin-flop takes place. In this case, spin-flip (not flop) transition happens, whereas one sub-lattice's magnetization reverses when $\vec{B}$ reaches a critical value, and the system's magnetic moments become aligned, resulting in a ferromagnetic state [6].

2.7.2 Antiferromagnetic ordering

Antiferromagnetic ordering can include several arrangements(Figure 3.17), with the end result being influenced only by the fact that amount of opposing moments has to be equal in both "up" and "down" positions. The number of these possible arrangements depends on the crystal lattice on which the moments are arranged. For FeRh, type G is the most common.

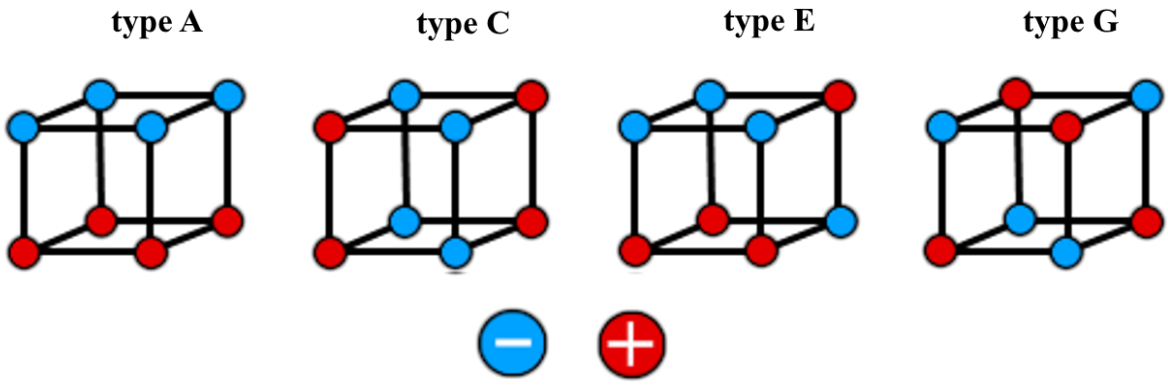

Figure 3.17: Different antiferromagnetic arrangements; red and blue denote different sub-lattice magnetization directions, with + (red) pointing upwards and - (blue) pointing downwards.

3 FeRh

FeRh alloy possesses unusual properties, namely the first order magnetic transition from anti-ferromagnetic (AF) to ferromagnetic (FM) state at a temperature of 370 K, which is also accompanied by a decrease of resistivity and expansion in the lattice parameter [10].

3.1 FeRh Alloys

In FeRh alloys, first order AF-FM transition take place only for rhodium concentrations within the range from 48% to 55%, with the concentrations closer to 50% showing a complete transition (Figure 3.18) [11]. Upon reaching the Curie temperature of the alloy, further ferromagnetic to paramagnetic transition occurs, this temperature lies in the vicinity of 670 K [11].

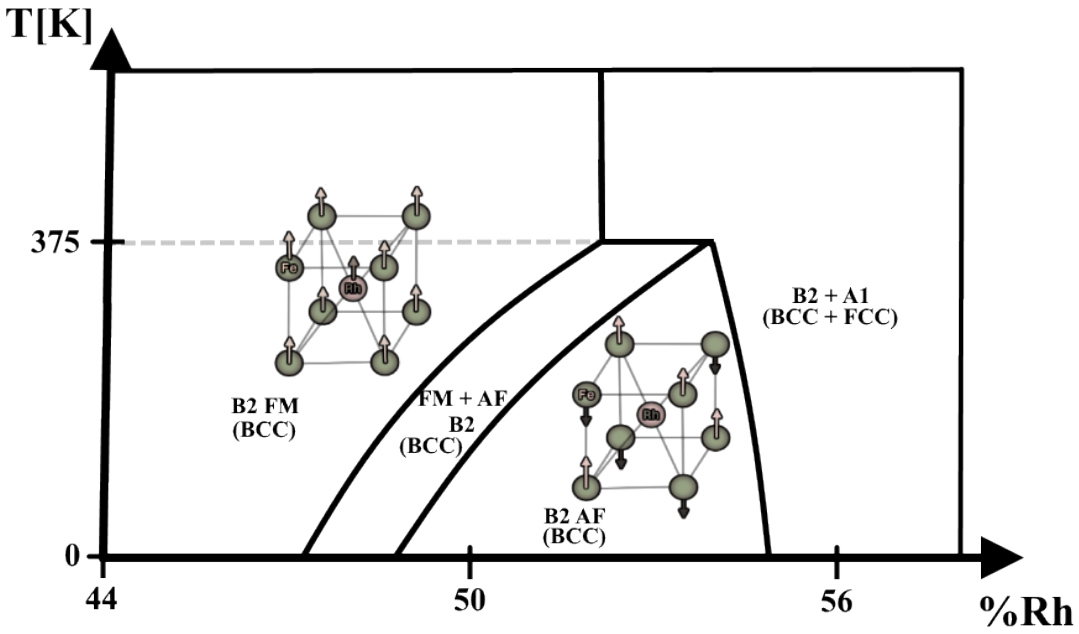

Figure 3.18: Close-up of FeRh phase diagram near 50% Rh concentration. Adapted with modifications from [11].

3.2 FeRh Structure

From the investigation by M. Vries, et al. [12] into the topic, it was determined that this transition for the described range of rhodium concentration ($48\% < x < 0.54\%$) is a magneto-structural one, meaning that the lattice constant value increases by approximately 0.3% in each linear dimension post-transition . The crystalline structure of this alloy is body-centered cubic, with Fe atoms occupying the corner positions (atomic position (0,0,0)), and Rh atoms occupying the central position (1/2,1/2,1/2) (Figure 3.18).

When in ferromagnetic state (above 370K) (Figure 3.18, B2 FM), the magnetic moments of both Fe and Rh had been measured to be $\mu_{Fe} = 3.2\ \mu_B$, and $\mu_{Rh} = 0.9\ \mu_B$ respectively [13,14]. When in anti-ferromagnetic state (Figure 3.18, B2 AF), magnetization contribution from Fe is $\mu_{Fe} = 3.3\ \mu_B$, while the contribution from Rh is $\mu_{Rh} = 0.8\ \mu_B$ [13].

3.3 FeRh phase transition

First order phase transition (Figure 3.19) is typical for all AF-FM transitions, during which coexistence of both phases is permitted (Figure 3.18, B2 FM + AF). The order parameter experiences a sudden change during the transition, which is related to change between zero and non-zero magnetization of the material (Figure 3.19) [3].

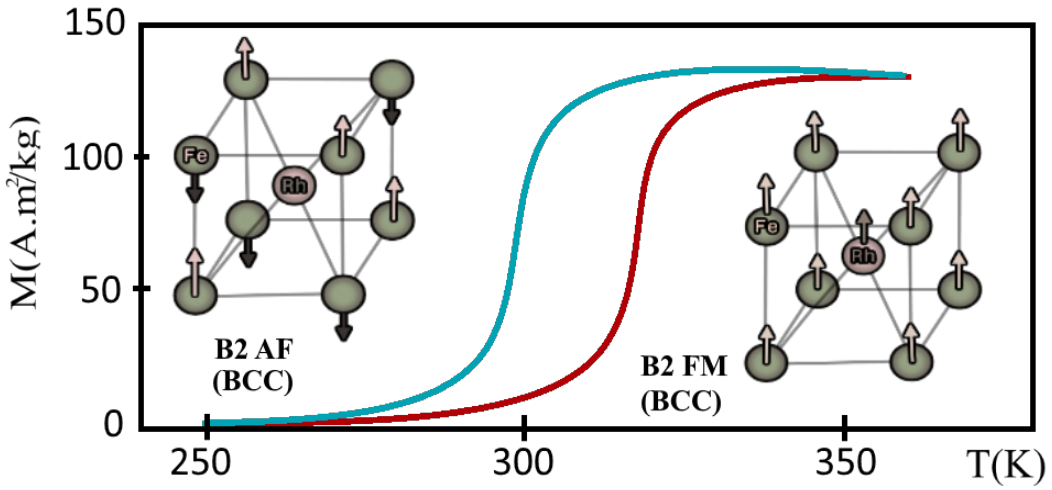

Figure 3.19: Fe Rh first-order phase AF-FM phase transition. Adapted from [15]

This transition can be influenced by external magnetic field, which, when applied, shifts the hysteresis loop to lower temperatures [15]. Mechanical pressure can also influence this transition temperature [16]. Furthermore, FeRh belongs in the category of alloys the magnetism of which is influenced by the degree of their chemical order. As the chemical order is decreased, the transition temperature shifts to a colder one [4,5].

The mechanism of the AF-FM phase transition itself was first theorized by Kittel, based on the relationship between lattice parameter and the value of exchange integral. However, later this model was proven to be false due to discrepancies between the total entropy and the change in lattice entropy during the transformation. Excess of entropy causes the ferromagnetic phase to be more stable than anti-ferromagnetic, which causes hysteresis [17].

3.4 FeRh thin films

For FeRh thin films, the crystalline structure is primarily governed by the substrate it is based on, with research done by Castiella, et al. [18] showing that the lattice parameter is influenced not only by the substrate on which the FeRh thin film is grown, but also by the deposition temperature (Figure 3.20).

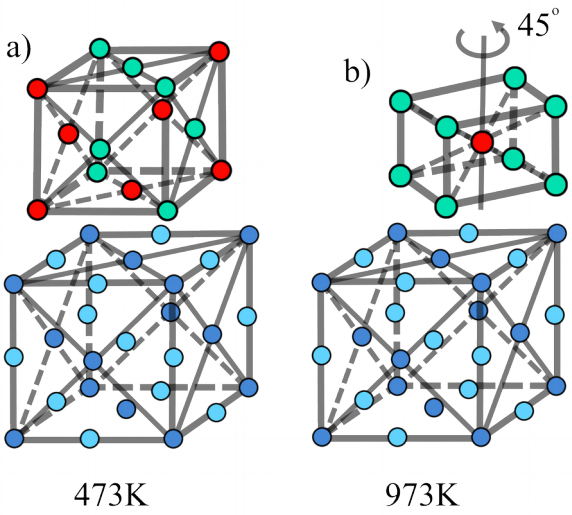

Figure 3.20: FeRh thin film growth as a function of temperature. light blue represents oxygen, dark blue represents magnesium, cyan represents iron, and red represents rhodium. Adapted from [18].

3.4.1 Ion irradiation of FeRh thin films

This section covers ion irradiation of FeRh thin films, including the basic principles behind ion irradiation as well as literature search regarding recent developments.

Ion-sample interaction

The basis of the ion irradiation principle, and how it affects the structure of thin films, is based around ion-sample collisions. These collisions are separated into elastic and inelastic collisions. The interaction is a function of energy, with nuclear interactions being significant at low ion energies, and electronic collisions being significant at high ion energies(Figure 3.21). The critical energy A at which the electronic interaction is more significant than nuclear is equal to the parameter A, the relative atomic mass of the ion [19].

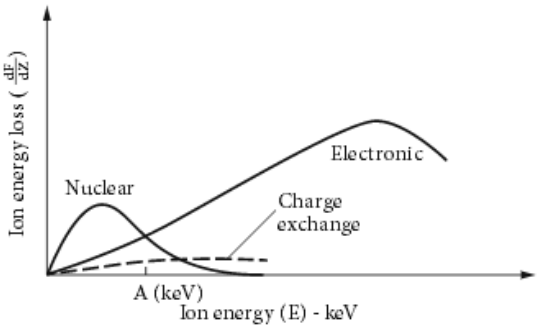

Figure 3.21: Energy loss as a function of ion energy., Taken from Frey, 2015, Particle Beam Sources.

The interaction which is of particular interest to us is the ion implantation. This interaction involves collision cascades, which create many dislocations as a mechanism of energy exchange between the fast moving ion and the material surrounding it, before finally being implanted (Figure 3.22) [19].This is one of the core mechanisms behind the ion irradiation-induced disordering, which is a method of thin film tuning that I investigated.

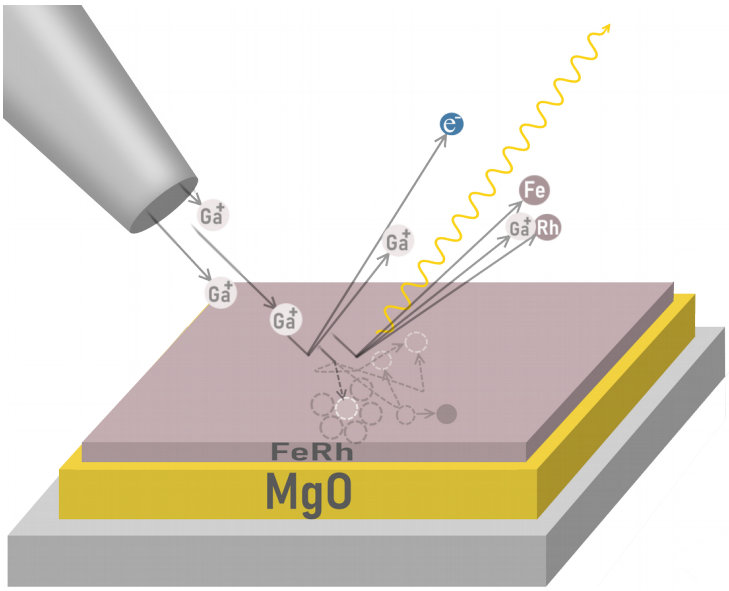

Figure 3.22: FeRh thin film ion irradiation by gallium ions. The interactions displayed are: back-scattering, charge transfer, milling, collision cascades, ion implantation. Adapted from[19].

FeRh thin film ion irradiation

K. Aikoh, et al. [20] investigated how 30 keV gallium ion irradiation affects AF-FM phase transition in FeRh thin film (30 nm). They confirmed that as a result of Ga ion irradiation there was a change in the phase transition, crystalline structure, as well as change in magnetic properties of the film at cryogenic temperatures. Furthermore, the experiments performed by A. Tohki, et al. [21] who used 50 keV argon ions, and 60 nm thick FeRh thin film showed converging data.

In another paper, investigated by K. Aikoh, et al. [22] they proved the viability of micrometer-scale ion microbeam magnetic structure patterning, using 10 MeV Iodine ions as their source, obtaining similar results to their work on full sample irradiation by 30 keV gallium ions.

FeRh thin film ion irradiated structure

X-ray diffraction scans for the initial and irradiated samples (Figure 3.23;3.24), showed slight decrease in B2 (BCC) crystalline structure (Figure 3.18) signal taking place up to 5 × 10^{13} ions/cm^2, after which the signal from B2 (BCC) structure started to decline rapidly, with the doses of 1 × 10^{14} Ions/cm^2 and upwards showing little to no signal from B2 (BCC) structure [20,21].

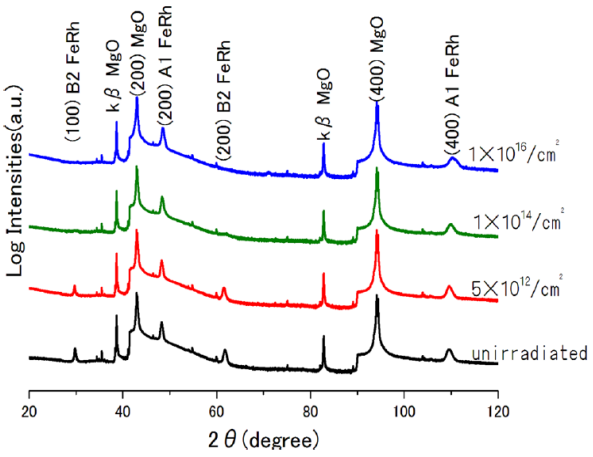

Figure 3.23: X-ray diffraction scan of FeRh thin film (60 nm) as a function of ion irradiation dose (50 keV, Ar).
(A. Tohki, et al. [21])

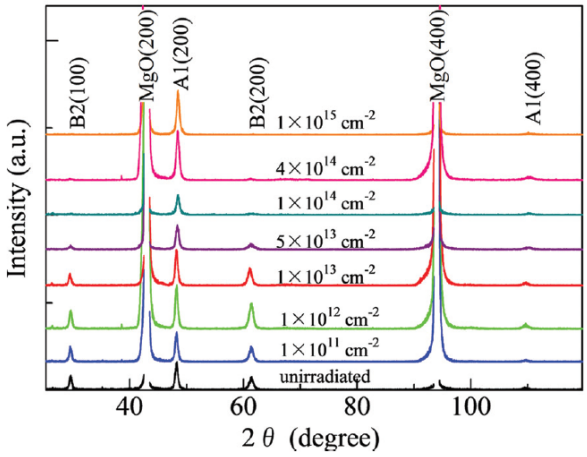

Figure 3.24: X-ray diffraction scan of FeRh thin film (30 nm) as a function of ion irradiation dose (30 keV, Ga).
(K. Aikoh, et al. [20])

Saturated magnetization of FeRh film after ion irradiation

Saturated magnetization increased with irradiation dose, reaching a maximum at 5 × 10^{13} Ions/cm^2 in the work done by K. Aikoh, et al.(Figure 3.26; 30 keV, Ga; 30 nm film), and reaching a maximum just below 1 × 10^{13} ions/cm^2 in the paper written by A. Tohki, et al.(Figure 3.25; 50 keV, Ar; 60 nm film). Beyond the maximum, the saturated magnetization starts to decline.

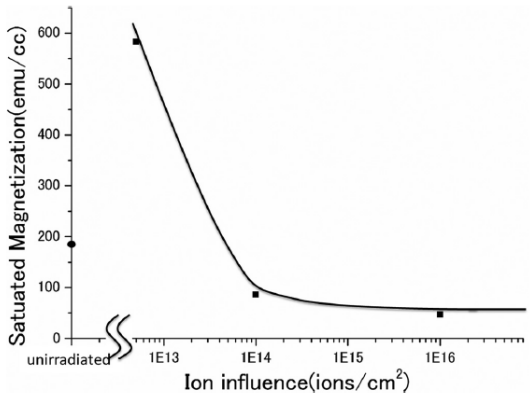

Figure 3.25: Saturated magnetization as a function of ion dose (50 keV, Ar; 60 nm film) .
(A. Tohki, et al. [])

FeRh thin film ion irradiated phase transition

In the research done by K. Aikoh, et al. [20], phase transition takes place only for ion doses lower than 5×10^{13} Ions/cm^2 , after which the hysteresis loop disappears completely, and the material behaves as a typical ferromagnet, with a drop in magnetization with increasing temperature (Figure 3.26, dose 1×10^{14} ions/cm^2). With the ion dose increasing even further to 4×10^{14} Ions/cm^2 and onwards, the behaviour can be considered paramagnetic in nature, with no pronounced drop of magnetization with temperature.

Unirradiated sample non-zero magnetization can be explained by the manufacturing process during which the defects are created within the thin film, which is related to FeRh sensitivity towards chemical ordering, which means that residual ferromagnetic phase is present [59].

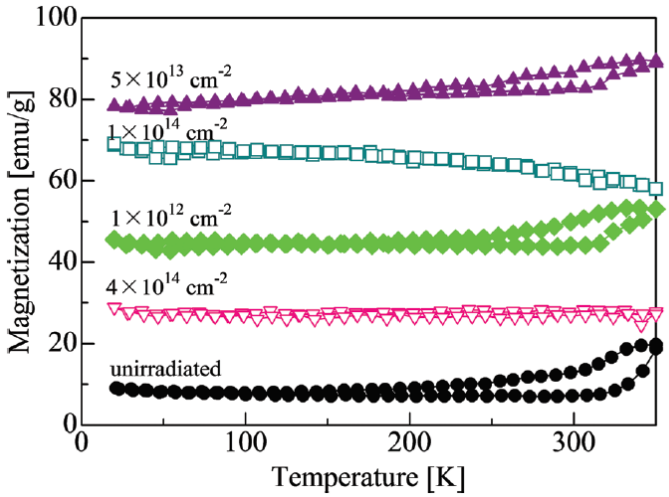

Figure 3.26: Magnetization of FeRh thin film as a function of temperature. Lower part of each loop is heating, upper part is cooling (30 keV, Ga; 30 nm film) (Aikoh, et al. [20])

FeRh thin film ion irradiation literature search summary

The presence of ferromagnetic behaviour from the disordering of the film increases saturated magnetization, which in turn enables the first-order phase transition to take place at lower temperatures, at the expense of the quality of this transition, making it less pronounced and more stretched, up to the point of disappearing completely [20].

3.4.2 Thermal annealing of FeRh thin films

A. Tohki, et al. [21] investigated how thermal annealing affects FeRh thin film irradiated by the ion dose of 1×10^{16} Ions/cm^2. In their case, as mentioned previously, the ion irradiation was performed using argon ions at 50 keV energy, the sample thickness was recorded to be 60 nm. Their results regarding the irradiation were quite similar to the ones in the work done by K. Aikoh, et al. [20], and we can safely assume that the ion irradiation dose of 1×10^{16} ions/cm^2 results in paramagnetic disordered state for FeRh thin films.

Thermal annealing principle

Thermal annealing of thin films can enable the diffusion, relaxation and recrystallization processes to take place within a reasonable time-frame. Depending on the conditions, annealing can help decrease the internal strain of newly-made epitaxial thin films. Ordinarily, the amount of internal defects decreases with annealing, which also corresponds to the increase of the grain size. However, for gold thin films, as a counter-example, research done by G.M. Alonzo-Medina et al. [23] shows that surface roughness increases alongside with grain size decrease as a function of annealing time (Figure 3.27), this relationship being logarithmic. The behaviour of grain size increase or decrease depends greatly on annealing temperature ramp as well as annealing time. This effect of different temperature ramps was also demonstrated by S.C. Chen, et al. [24] using FePt thin films.

Annealing temperature can also affect thin films by enabling surface tension to overtake internal forces, causing porosity, or nucleation of blobs to occur. One of such FeRh thin films which was prepared by my colleague M.Sc. Jon Ander Arregi Uribeetxebarria, showed such behaviour, known as dewetting (Figure 3.28).

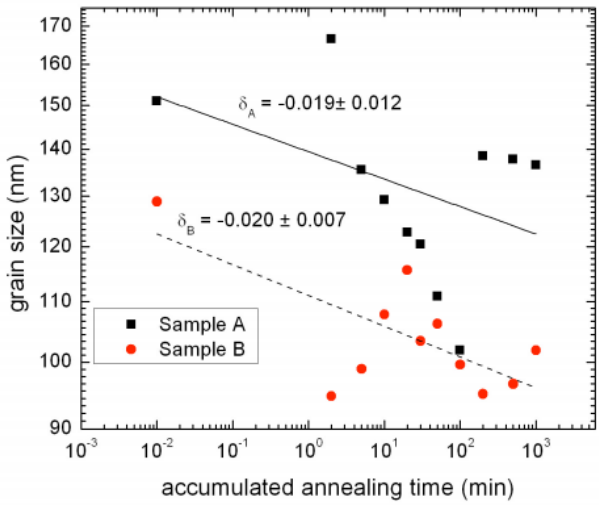

Figure 3.27: grain size as a function of annealing time, Au thin film. Taken from [23]

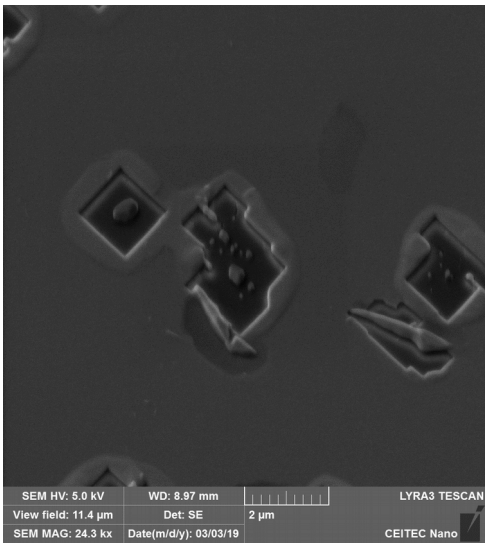

Figure 3.28: SEM scan of FeRh thin film defects caused by thermal annealing (55° inclined)

Influence of thermal annealing on FeRh thin film structure

In their investigation into FeRh thin film annealing, A. Tohki, et al. [21] demonstrated that annealing of ion irradiation disordered (1×10^{16} Ions/cm^2) FeRh thin films does restore the previously vanishing body-centered cubic B2 structure. However, they were also able to show that annealing from the ion irradiation dose of 1×10^{16} ions/cm^2 does not show any significant restructuring taking place if the sample is annealed at a temperature lower than 200°C (Figure 3.29).

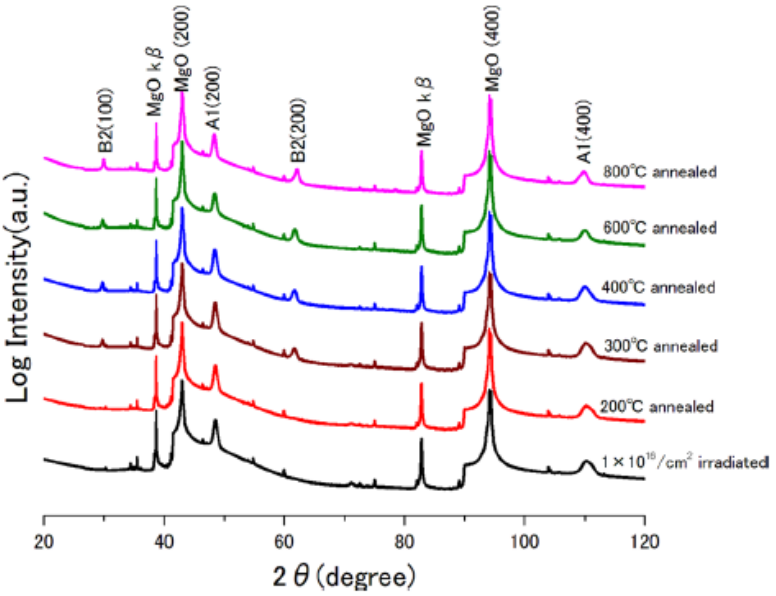

Figure 3.29: X-ray diffraction measured structure after each annealing temperature (50 keV, Ga; 60 nm thick film [21]).

Influence of thermal annealing on FeRh thin film magnetization

A. Tohki, et al. [21] have also demonstrated that in-line with the restoration of structural properties, the magnetic properties are also restored gradually with an increase of the annealing temperature (Figure 3.30). This corresponds to the maximum saturated magnetization achieved after annealing at a temperature close to 400°C, and with partial restoration of AF behaviour at annealing temperatures greater than 400°C, with near-complete restoration of the antiferromagnetic state prior to irradiation appearing near 800°C.

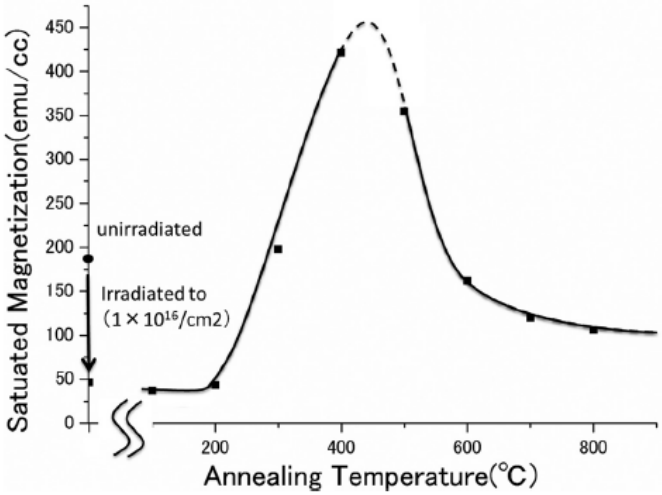

Figure 3.30: Saturated magnetiyation as a function of annealing temperature, measured at 5K (50 keV, Ar; 60 nm thick film. Taken from [21])

Influence of thermal annealing on FeRh thin film phase transition

In the same vein, A. Tohki, et al. [21] discovered that annealing affected the thin film behaviour in a manner opposite to ion irradiation(Figure 3.31). The maximum saturated magnetization correlates with fully ferromagnetic behaviour of the material in question, being in good agreement with the research done by K. Aikoh, et al. [20].

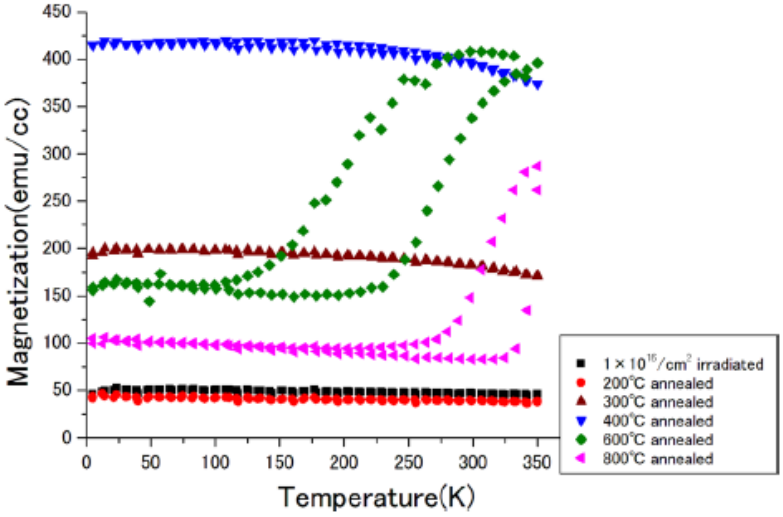

Figure 3.31: Magnetization as a function of temperature, measured at 5K. (50 keV, Ga; 60 nm thick film. Taken from [21]).

FeRh thin film thermal annealing literature search summary

FeRh thin film properties can be modified in a manner opposite to ion irradiation by thermal annealing. However, caution must be taken in the following of the proper regime for annealing in order to avoid unfortunate destruction of the thin film.

Furthermore, grain size and annealing temperature relationship in FeRh thin films is unclear, possibly limiting the overall number of cycles that can be achieved via repeated ion irradiation and annealing, warranting further literature search on this topic [23,24].

4. Methods and Experiments

This section will go over methods and instruments used as well as experiments designed for the testing of magnetic properties of the locally ion-irradiated and thermally annealed FeRh thin film.

4.1 Instruments

This section will go over the instruments used in the course of my research into the topic, going over the principles at work of Scanning Electron Microscope(SEM), Focused Ion Beam(FIB) with a Liquid Metal Ion Source(LMIS). Atomic Force Microscopy(AFM) will also be covered, including different modes of operation that were used during the course of this work in order to evaluate the magnetic field of the irradiated areas on FeRh thin film.

4.1.1 Vacuum scanning electron microscope

Scanning electron microscope creates magnified images of a sample by the means of a focused beam of electrons scanning over the surface of the sample. The electrons interact with the sample (Figure 4.1), as a result of which the secondary electrons, back-scattered electrons, Auger electrons, as well as characteristic, fluorescent and continuum X-rays are produced. Imaging is done primarily by using secondary and back-scattered electrons, although chemical imaging is also possible by using an appropriate Auger electron detector [25]. Similarly, the generated X-rays can also be used for chemical imaging using a method called energy-dispersive X-ray spectroscopy [26].

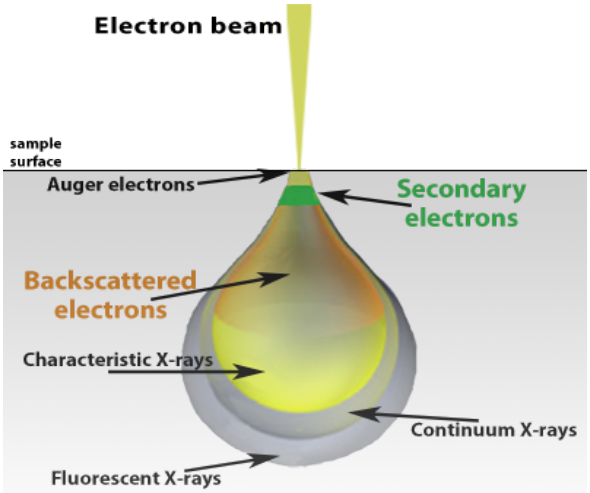

Figure 4.1: Possible interactions between the electron beam and the surface

Electron gun, which is situated at the top of the column(Figure 4.2), is a source of electrons which are then accelerated via a series of electromagnetic lenses. The lenses then focus the beam of electrons. The beam of electrons is controlled by the deflection coils which perform the scanning of the sample surface.

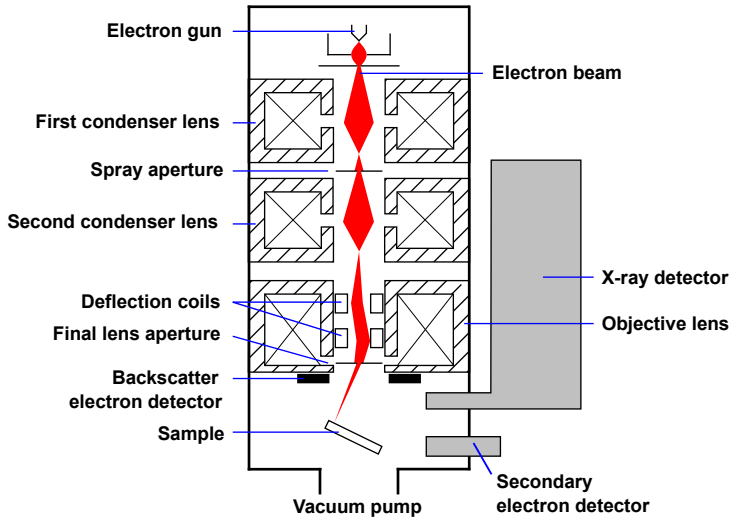

Figure 4.2: Typical construction of a SEM. Taken from commons.wikimedia.org/wiki/File:Schema_MEB_(it).svg

3.1.2 Vacuum focused ion beam

In our case, a Liquid Metal Ion Source (LMIS) Focused Ion Beam (FIB) was used (Figure 4.3). One of the main reasons being availability, but also convenience due to the fact that it is paired up with a scanning electron microscope, allowing us to direct the FIB without having to bombard the surface with ions. It also operates at lower energies than gas field ionization source, has less penetrative ability, and also allows for smaller spot sizes [27].

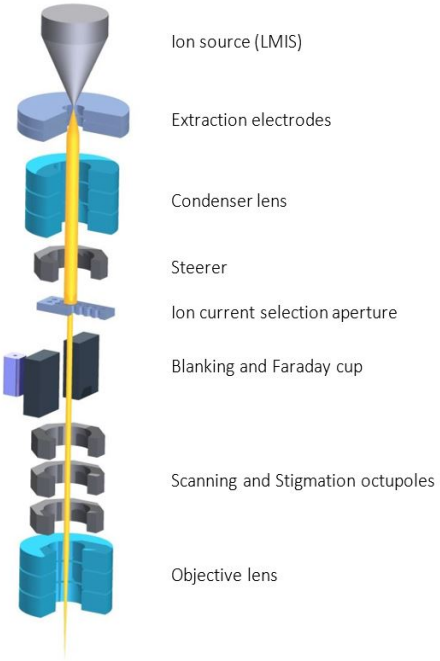

Figure 4.3: LMIS FIB internal structure. Taken from: orsayphysics.com/what-is-fib

Heated gallium wets the tungsten needle and flows to the tip, where surface tension and electric field form the gallium into a Taylor cone (Figure 4.4). The electric field, which is greater than 10^8 V/cm, causes ionization and field emission of the gallium ions. Ions are then can be accelerated to an energy of 1 to 30 keV, and focused onto the sample by the means of electrostatic lenses.

FIB can also be used for imaging, as the collisions emit secondary electrons which can be

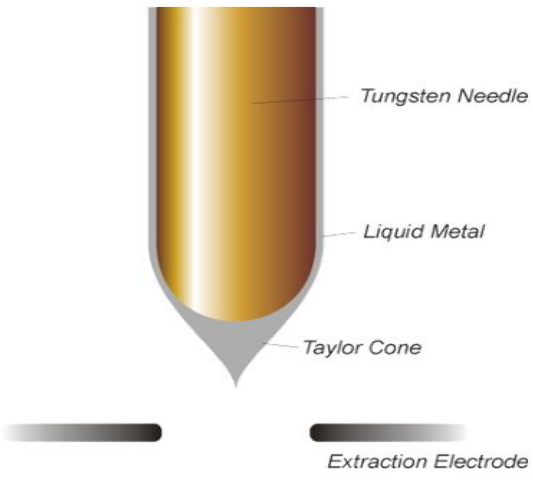

Figure 4.4: Liquid Metal Ion Source (LMIS) needle.
Taken from http://www.orsayphysics.com/what-is-fib

detected following a similar principle as seen in SEM. It is significantly more destructive during continuous scanning, making it unusable for long exposure, high magnification observations.

3.1.3. Atomic Force Microscope

Atomic Force Microscope, also known as Scanning Force Microscope, is a high resolution measurement instrument, which allows for the recording of topography of a surface. Its special resolution is superior compared to optical microscopy, allowing for sub-nanometer resolution [28]. It works on principle of measuring force interactions between the probe and a sample. The force interactions between the tip and the sample include: strong force, Van deer Waals forces, dipole-dipole interactions, electromagnetic and electrostatic forces, as well as other interactions.

In order to scan the surface, a very sharp tip located at the end of a cantilever is used as a probe, which is then controlled by piezoelectric elements in 3 axes. In our case, optical detector is used: the cantilever's surface which is opposite to the tip is polished, so that the laser can be directed at it. The reflected signal is collected at a 4-part photosensitive detector, which converts light into electric potential (Figure 4.5). This gives us the information as to the movement of the tip relative to its starting position, indicating a change in amplitude of periodic oscillations, or deflection, depending on the mode of operation. It also allows to see the changes in torsion, thanks to 4-part detector which registers to which quadrant the shift occurs.

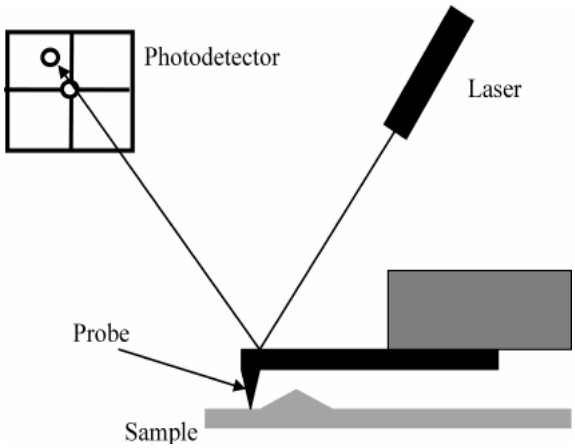

Figure 4.5: AFM with laser detector setup

Contact mode

In this mode the tip stays in contact with the sample as it is moving across the surface (Figure 4.6). In order to avoid undesired effects of the tip “sticking” to the sample, considerable deflection of the cantilever has to be used in order for the forces between the tip and the sample to be predominantly repulsive. The measurement can be conducted either from the deflection of the cantilever directly, or, when a more gentle approach is desirable, using a feedback loop which keeps the deflection constant at the expense of the probe’s positioning in the z-axis. It is also worth mentioning that when scanning samples with very pronounced topography and low mechanical resistance, scarring can occur.

Tapping mode
In this mode of operation, instead of keeping the tip in the contact with the surface features of the sample, the cantilever with the tip is instead oscillated near its resonant frequency, with an amplitude equal to the distance between the tip and the sample in the initial position (Figure 4.7). In this case, the tip is more sensitive to sharp topographical features. The change in amplitude, caused by a change of distance between the set point and the surface is then registered by the feedback loop, and the cantilever-sample distance is adjusted so that the amplitude prior to this change is achieved.

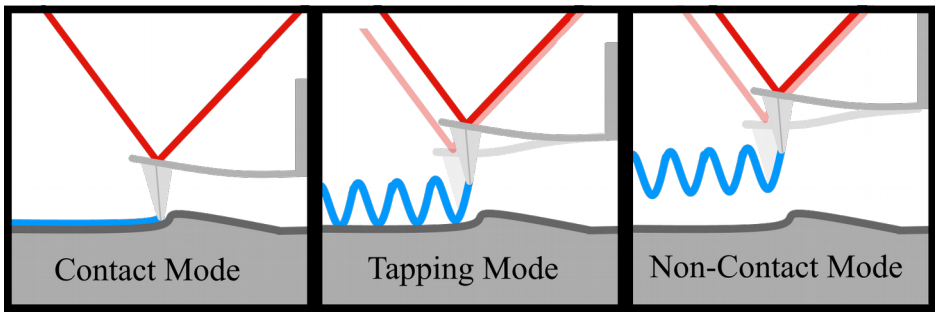

Figure 4.6: Different scanning modes

Non-contact mode
It is similar in principle to the tapping mode, but in this case, the tip does not directly interact with the surface, limiting the force interactions only to relatively long-range forces, such as electrostatic and electromagnetic forces (Figure 4.6). As in the previous case, the change in amplitude of oscillations is measured, and the feedback loop is used to return to the original value of the amplitude.

Magnetic force microscopy
Magnetic Force Microscopy (MFM), in our case, combines non-contact and tapping modes, in so-called lift mode (two-pass imaging), where the first pass is done measuring the topography, and the second pass is done oscillating the needle at a higher altitude (to avoid surface interactions), replicating the previously scanned terrain and registering the tip attraction or repulsion relative to the previous data.

In order to measure the magnetic response from the sample, the tip used for this scanning mode should be magnetic (typically Si tip with a thin magnetic coating). The sample can also be placed in an external magnetic field in order to align the magnetization direction, and make evaluation easier.

4.1. Deposition of FeRh thin film

Deposition of FeRh thin film was performed by Bc. Lucie Motyčková using magnetron sputtering. The deposition took 8 minutes at 450 °C, nominal thickness was 16 nm. Post-deposition sample was annealed for 80 minutes at 760°C under high vacuum.

In a magnetometry measurement performed by my supervisor, Dr. Ing. Michal Staňo, the transition temperature for the film is shown to be above 400 K, especially considering that it was measured in an external magnetic field of 3 Tesla (Figure 4.1).

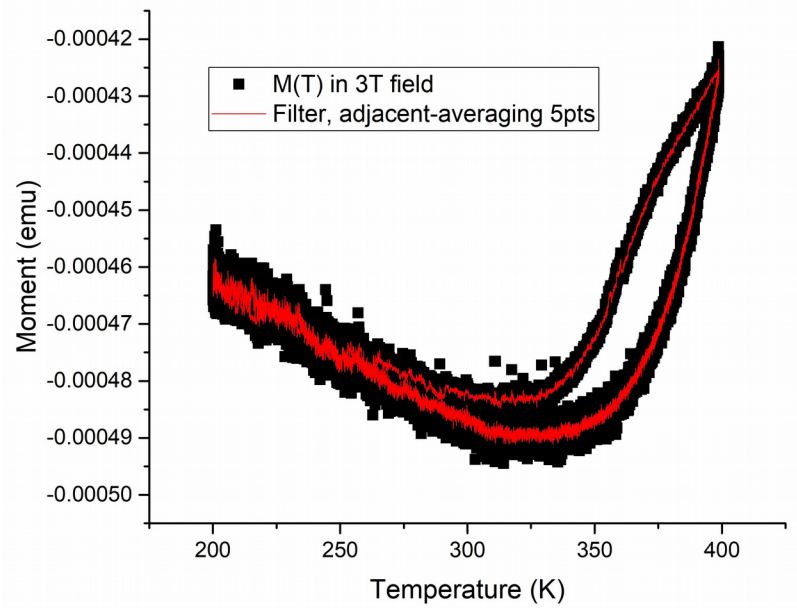

Figure 4.7: Initial phase transition measurement for the FeRh thin film (16 nm)

4.2 Local ion irradiation of FeRh thin film

An array of 2 × 2 μm squares for FIB irradiation was created using Atlas DrawBeam software (Figure 4.8), with following doses:

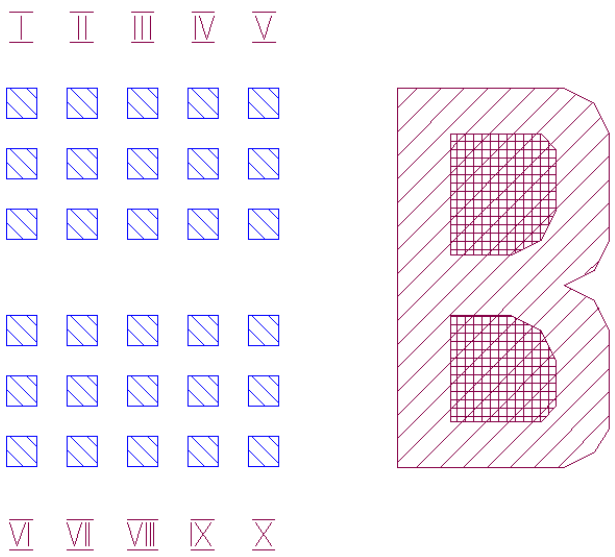

Column	Ions/cm^2
I	1×10^{11}
II	5×10^{11}
III	1×10^{12}
IV	5×10^{12}
V	1×10^{13}
VI	5×10^{13}
VII	1×10^{14}
VIII	5×10^{14}
IX	1×10^{15}
X	5×10^{15}

Figure 4.8: Focused Ion Beam irradiation patterns

The irradiation was performed using Tescan Lyra scanning electron microscope with an installed Gallium-based LMIS FIB under high vacuum. AFM and MFM measurements were performed using the Bruker Dimension Icon atomic force microscope. Heating of the sample was performed using custom-built heating stage using peltier cells.

4.1 Thermal annealing of FeRh thin film

Thermal annealing was performed by my supervisor Dr. Ing. Michal Staňo at a temperature of 410°C, for a period of 70 minutes in a preparation chamber (Scienta Omicron nanoSAM instrument) under initially ultra high vacuum (less than 10^{-5} Pa).

5. Results & Discussion

5.1 Locally ion-irradiated FeRh thin film

This section will go over the obtained measurements of FeRh thin film which underwent local ion irradiation by FIB using Gallium ions.

5.1.1 AFM measurement of the structure

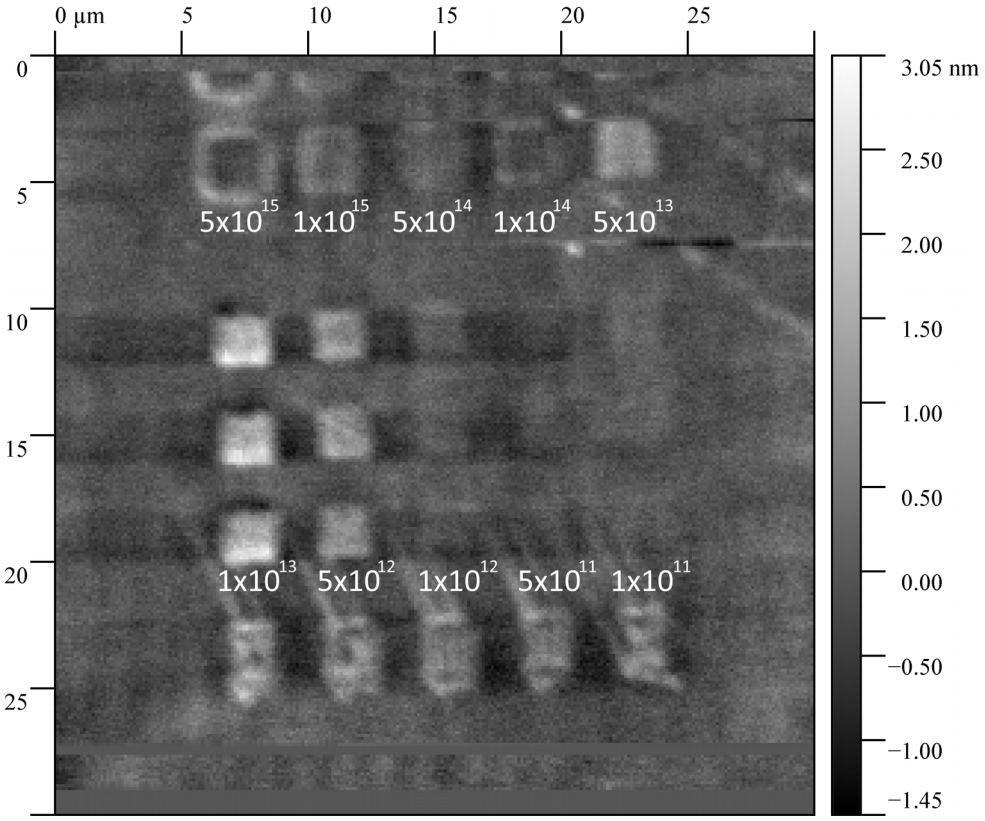

Figure 5.1: Topograhy measured by AFM measurement of locally FIB-irradiated FeRh thin film, 16 nm thick on MgO substrate.

For the lower doses, namely 1×10^{11}, 5×10^{11}, and 1×10^{12} ions/cm^2 no significant topography was measured. For higher doses, namely 5×10^{12}, 1×10^{13}, and 1×10^{14} ions/cm^2, an increase in topography of a few nanometers can be observed. This is very likely related to the swelling effect connected to the phenomenon of Gallium ion implantation in the MgO substrate [29], as the film manufactured was noticeably thinner than originally planned for, meaning that more significant amount of ions was implanted into the substrate. For even higher doses, namely 5×10^{14}, 1×10^{15}, and 5×10^{15} ions/cm^2, a decrease in topography can be seen, corresponding to the milling of the thin film starting to occur at the doses of 5×10^{13} up to 5×10^{15} ions/cm^2 . The rise of elevation around the ion irradiation dose of 5×10^{15} ions/cm^2 could represent re-deposition effect, or the residual swelling of the substrate, or the combination of the two. The effects of thin film milling and MgO substrate swelling can combine, diminishing the milled depth.

5.1.2 MFM measurement of the magnetic response

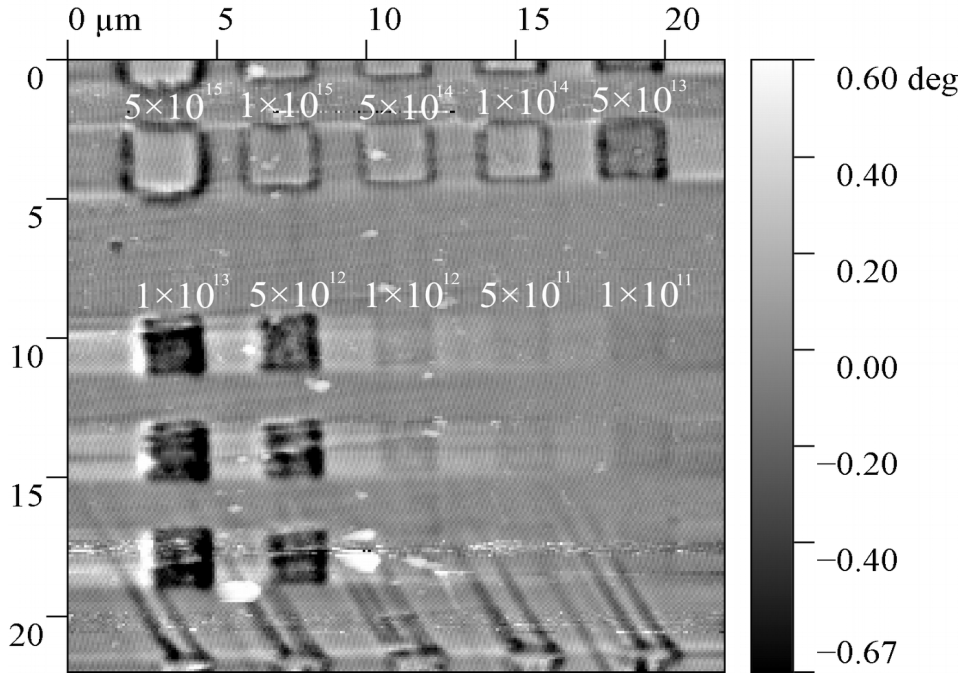

Figure 5.2: MFM ion irradiated sample measurement performed at 20 ℃

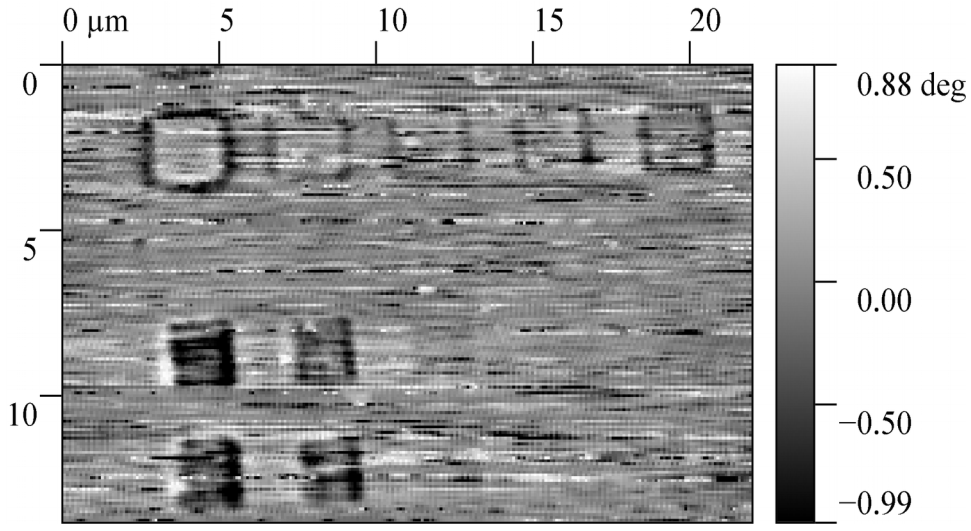

Figure 5.3: MFM ion irradiated sample measurement performed at 40 ℃

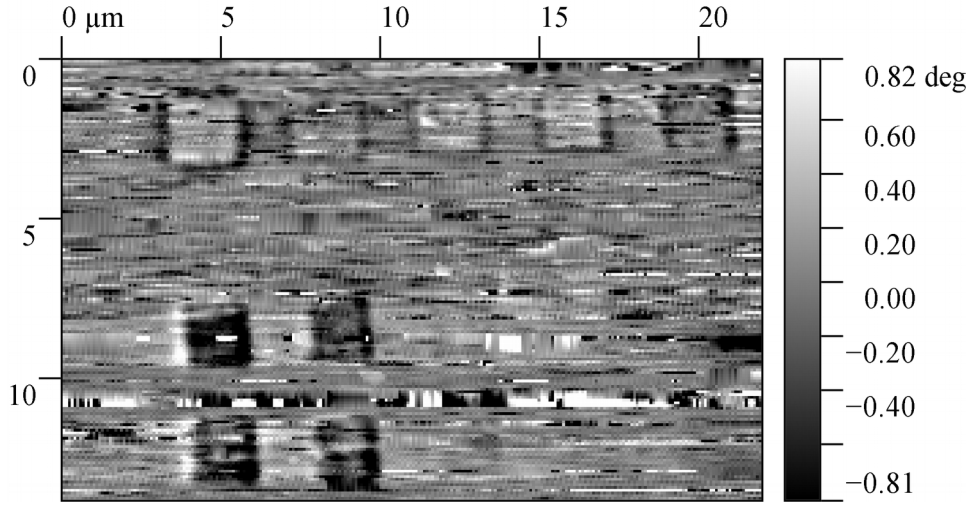

Figure 5.4: MFM ion irradiated sample measurement performed at 60 ℃

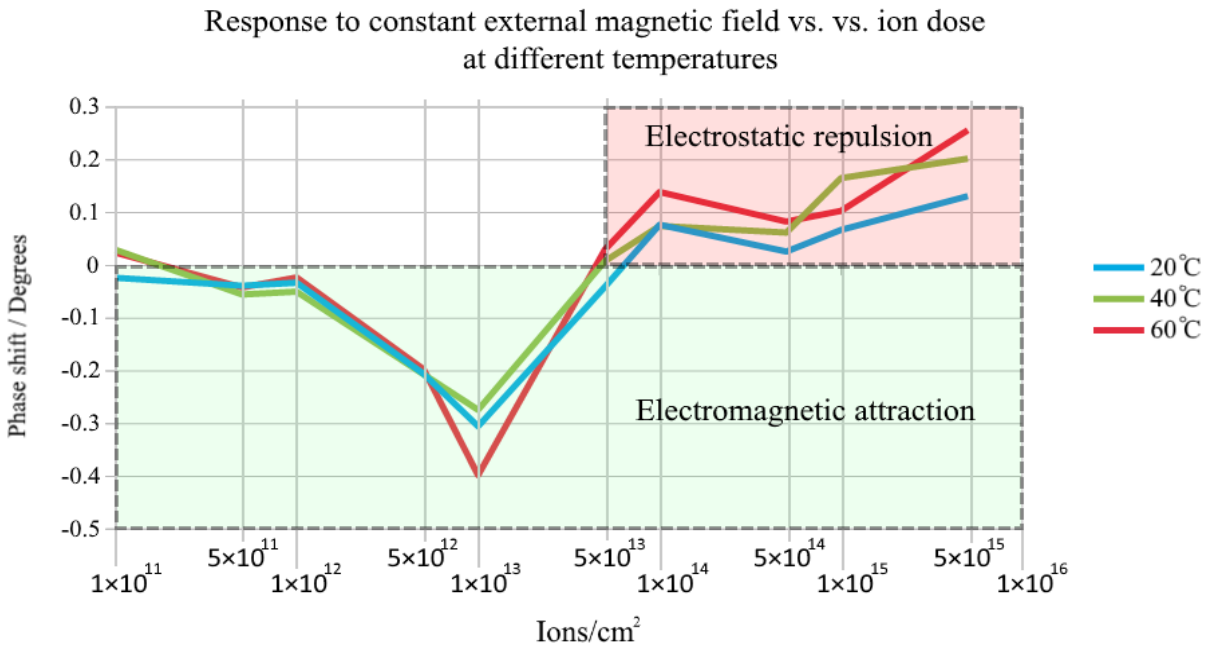

Figure 5.5: Magnetic response from the irradiated areas as a function of ion dose and temperature.

For the lower doses at 20°C (Figure 5.2), namely 1×10^{11}, 5×10^{11}, and 1×10^{12} ions/cm^2, the magnetic response is attractive (negative) and weak, and with increasing temperature it appears to stay more or less constant.

For the area dose values of 5×10^{12} and 1×10^{13} ions/cm^2, strongest magnetic response can be observed among all irradiated areas. The vertical edges of these areas also show bright and dark contrast, indicating in-plane part of the magnetization of the area. With increasing temperature, the area dose of 1×10^{13} ions/cm^2 demonstrates an increase in the value of phase shift, indicating that the attraction is stronger at higher temperature (Figure 5.5). This can be explained by first order phase transition taking place, where the antiferromagnetically ordered part of the thin film begins it's transition to ferromagnetic state at a lower temperature than the sample. This converges with the research done by both A. Tohki, et al. and K. Aikoh, et al. [20,21], where they received similar behaviour for the values of $\sim5\times10^{12}$ ions/cm^2 and $\sim5\times10^{13}$ ions/cm^2 respectively.

For even higher doses, namely 1×10^{14}, 5×10^{14},1×10^{15} and 5×10^{15} ions/cm^2, we receive a positive response irrespective of temperature, signifying that repulsion is taking place (Figure 5.2; 5.3; 5.4). Given that this value is well above background, it is likely to be due to electrostatic charging of the substrate or of the disordered FeRh thin film, making evaluation of magnetic response complicated for higher doses.

The spots which quantitatively represent the strongest magnetic attraction of the cantilever tip to the sample are represented as borders of the areas irradiated by the doses of 1×10^{14}, 5×10^{14}, 1×10^{15} and 5×10^{15} Ions/cm^2 (Figure 5.2;5.3;5.4). This behaviour can be mostly attributed to the FIB partially irradiating the sample near the border, but it could also be connected to the interfacing of disordered paramagnetic phase and ordered anti-ferromagnetic phase, though this cannot be confirmed as the measurement of higher doses were inconclusive due to electrostatic repulsion.

5.2 Thermally annealed FeRh thin film

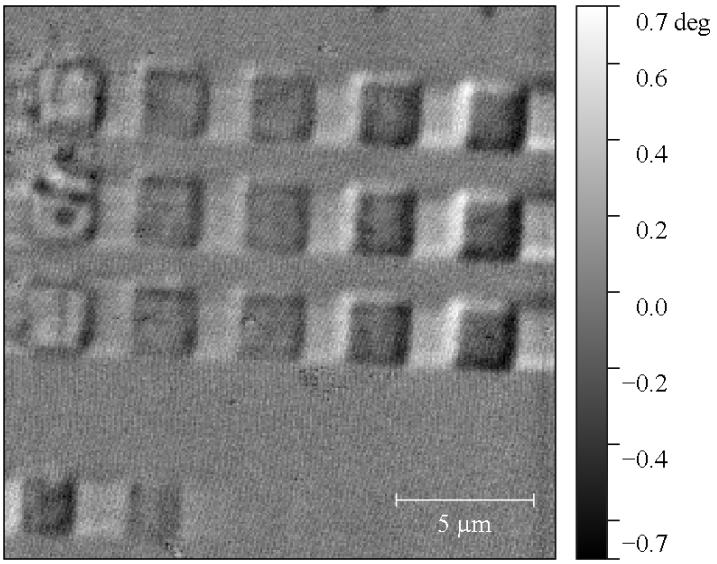

Figure 5.6: MFM measurement of the irradiated and annealed FeRh thin film at 20°C

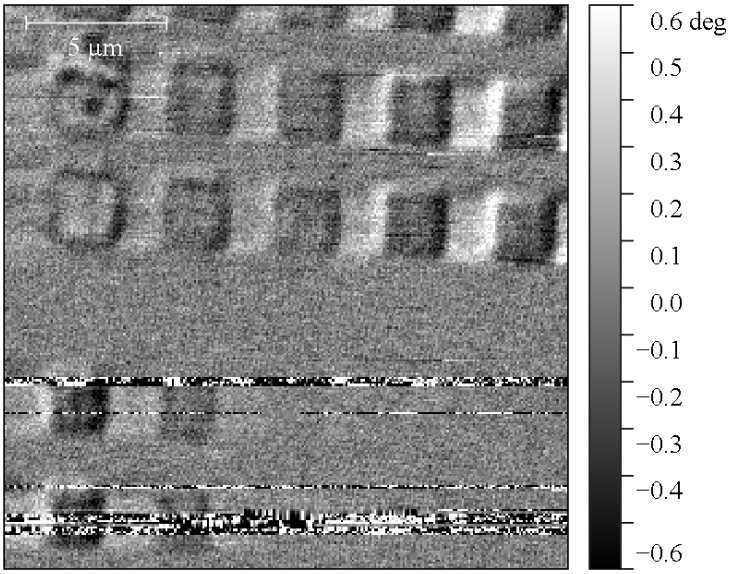

Figure 5.7: MFM measurement of the irradiated and annealed FeRh thin film at 20°C

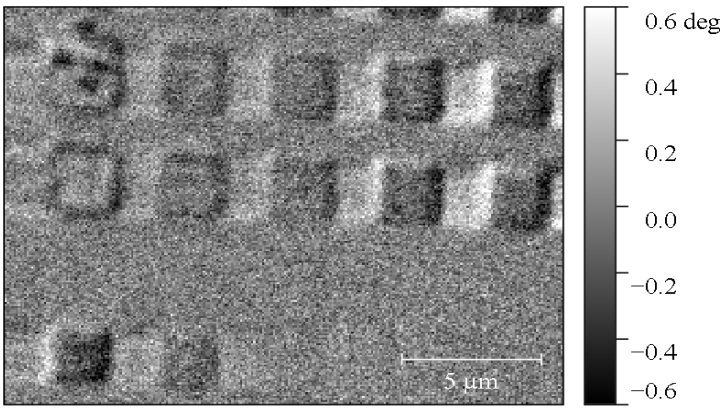

Figure 5.8: MFM measurement of the irradiated and annealed FeRh thin film at 20°C

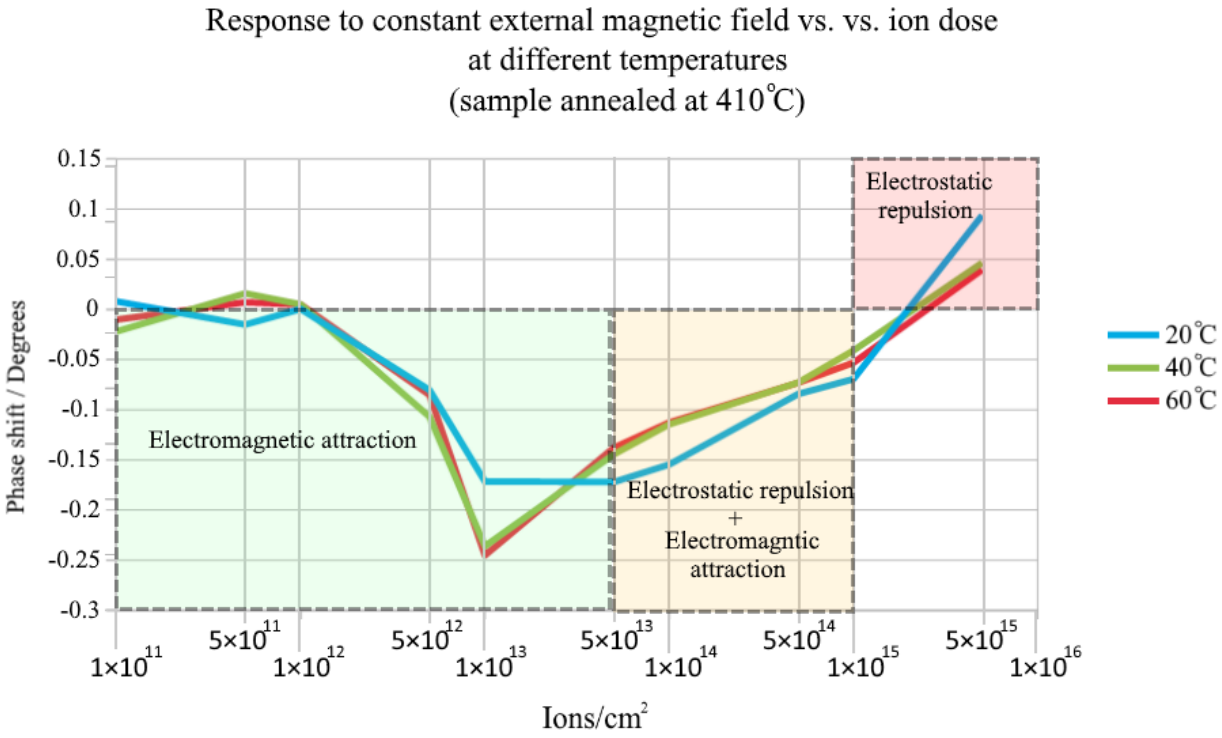

Figure 5.9: Magnetic response from the irradiated and thermally annealed areas as a function of ion dose and temperature.

For the most magnetically pronounced doses of 5×10^{12} and 1×10^{13} Ions/cm^2, it is hard to evaluate if there is any significant difference at room temperature for pre- and post-annealed sample, as the conditions were different, so was the magnitude of the phase shift (Figure 5.9). However, temperature-dependent behaviour shows that the first order phase transition does take place within our range of measured temperatures. Moreover, the magnetic response difference between measurement taken at 40°C and 60°C is minimal, signifying that the thin film irradiated with ion dose of 1×10^{13} ions/cm^2 and annealed at a temperature of 410°C largely finished its first-order phase transition before it was heated to the temperature of 60°C (Figure 5.9).

For the more irradiated areas, namely 1×10^{14}, 5×10^{14} and 1×10^{15} ions/cm^2,which previously were obscured by repulsive forces, are now clearly observed enacting an attractive force upon the tip (negative response). Given this change in behaviour across all highly irradiated areas, this is likely the signifier that annealing had an effect in restoring their structure from the disordered state, to body-centered cubic ferromagnetic, similar to what A. Tohki, et al. [21] have observed. Diffusion could play a role during the annealing of the sample, as the relaxation could occur in the substrate, causing a decrease in repulsive forces.

However, the highest irradiation dose of 5×10^{15} ions/cm^2 still interacts in a mostly repulsive manner with the MFM tip, showing that the electrostatic contribution is likely still present across all areas of higher (5×10^{13} to 5×10^{15}) irradiation doses to some extent (Figure 5.8). It also shows strong ferromagnetic response not only on the border of the square, but also within the square in the shape of grains and lines, signifying that even for the highest irradiation dose, there was a

change of structure and magnetic properties post-annealing. Whether it was partial or complete is hard to evaluate.

6. Conclusions

This work focused on on literature review and experimental evaluation of local ion irradiation and thermal annealing as a method for tuning the phase transition and magnetization of FeRh thin films.

In the literature, the magnetic properties and transition temperature of FeRh thin film varies with the ion dose [20]. For the case of 30 keV, gallium FIB and 30 nm thick FeRh thin film, and the doses up to 5×10^{13} ions/cm^2, the phase transition moved to lower temperatures, and saturated magnetization increases at low temperatures. The maximum saturated magnetization was achieved at ion dose of 5×10^{13} ions/cm^2. Here, the phase transition was faint, and it disappeared completely at a dose of 1×10^{14} ions/cm^2; the material was fully ferromagnetic and saturated magnetization was decreasing with temperature. At even higher irradiation doses, the material was paramagnetic. A. Tohki, et al. [21] observed an increase in saturated magnetization with ion irradiation dose up to, roughly 5×10^{12} ions/cm^2.

Annealing of an excessively-irradiated FeRh thin film (1×10^{16} ions/cm^2) showed that with the increasing temperature, the film first obtains ferromagnetic behaviour (up to 400°C), and with an even further increase it would obtain its original antiferromagnetic phase (up to 800°C).

Our experiments consisted of local ion irradiation (2 × 2 μm squares) of 16nm-thick film using 30 keV Ga FIB with doses ranging from 1×10^{11} ions/cm^2 to 5×10^{15} ions/cm^2. Irradiated (and later annealed) areas were probed by magnetic force microscopy in constant magnetic field at different temperatures. Due to the sample's relatively high phase transition temperature (above 400K), the full transition curve could not be measured. However, we did obtain data for temperatures from 20°C to 60°C. The irradiated sample was measured again after annealing at 410°C, which corresponds to the maximum saturated magnetization for an irradiated film as reported by A. Tohki, et al. [21].

For our conditions (30 keV gallium FIB, film thickness 16 nm, locally irradiated 2 × 2 μm squares) the maximum saturated magnetization ion dose was determined to be 1×10^{13} ions/cm^2. Highly ferromagnetic borders around irradiated areas were formed for doses above 5×10^{13} ions/cm^2. After the annealing, we obtained an increase of ferromagnetic response across higher irradiation doses (5×10^{13} ions/cm^2 up to 5×10^{15} ions/cm^2), with a possible slight decrease for the ion doses of 1×10^{13} Ions/cm^2 and less, signifying a possible partial restoration of the AF phase.

As a result of the experiments, we have qualitatively confirmed the validity of work done by K. Aikoh, et al. [20] as well as A. Tohki, et al. [21] regarding FIB irradiation and annealing of FeRh thin films. For further experiments, the FeRh thin film should have a greater thickness to prevent MgO substrate from swelling and charging, ideally the thickness should be close to 27 nm, as simulated in SRIM 2008 code. Greater care should be exercised during the irradiation process, especially calibrating the actual FIB spot size and the one selected in the software, to avoid unfortunate situations where instead of an irradiated area, an array of irradiated dots is created.

In order to expand on this research in quantitative manner, greater variety of doses should be used, but most importantly the sample should have transition temperature around 370K so that the whole transition can be verified for each dose. Polarized light optical microscope was considered for the measurements, but unfortunately the structures were not discernable. For larger structures this should not pose a problem. Temperature drift largely did not pose a problem during our MFM measurements, but it may have influence at higher temperatures. Additionally, investigating the structures of varying size and shape could also prove useful.

7 Bibliography

(1) Fallot, M.,& Hocart, R. (1939). Sur l'apparition du ferromagnétisme par élévation du température clans des alliages de fer et de rhodium. *Revue Scientifique, 77*, 498.

(2) Vegerhof, A., Barnoy, E., Motiei, M., Malka, D., Danan, Y., Zalevsky, Z., & Popovtzer, R. (2016). Targeted Magnetic Nanoparticles for Mechanical Lysis of Tumor Cells by Low-Amplitude Alternating Magnetic Field. *Materials,9*(11), 943. doi:10.3390/ma9110943

(3) Blundell, S. J., & Blundell, K. M. (2009). Phase transitions. *Concepts in Thermal Physics,* 321-344. doi:10.1093/acprof:oso/9780199562091.003.0028

(4) Bali, R., Wintz, S., Meutzner, F., Hübner, R., Boucher, R., Ünal, A. A., . . . Fassbender, J. (2014). Printing Nearly-Discrete Magnetic Patterns Using Chemical Disorder Induced Ferromagnetism. *Nano Letters,14*(2), 435-441. doi:10.1021/nl404521c

(5) Zeng, Q., & Baker, I. (2006). Magnetic properties and thermal ordering of mechanically alloyed Fe–40at% Al. *Intermetallics, 14*(4), 396-405. doi:10.1016/j.intermet.2005.07.005

(6) Blundell, S., & Thouless, D. (2003). Magnetism in Condensed Matter. *American Journal of Physics,71*(1), 94-95. doi:10.1119/1.1522704

(7) Langevin, P. (1905). Sur la théorie du magnétisme. *Journal de Phzsique Théorique et Appliquée. d*oi:10.1051/jphysta p:019050040067800&lang=fr (inactive 6 September 2018), ISSN 0368-3893.

(8) Diamagnetism Of Metals. (1965). *Collected Papers of L.D. Landau,* 31-38. doi:10.1016/b978-0-08-010586-4.50009-2

(9) Kittel, C., & Hellwarth, R. W. (1957). Introduction to Solid State Physics. *Physics Today, 10*(6), 43-44. doi:10.1063/1.3060399

(10) Zsoldos, L. (1967). Lattice Parameter Change of FeRh Alloys due to Antiferromagnetic-Ferromagnetic Transformation. *Physica Status Solidi (b), 20*(1). doi:10.1002/pssb.19670200148

(11) Swartzendruber, L. J. (1984). The Fe−Rh (Iron-Rhodium) system. *Bulletin of Alloy Phase Diagrams,5*(5), 456-462. doi:10.1007/bf02872896

(12) Vries, M. A., Loving, M., Mihai, A. P., Lewis, L. H., Heiman, D., & Marrows, C. H. (2013). Hall-effect characterization of the metamagnetic transition in FeRh.*New Journal of Physics, 15*(1), 013008. doi:10.1088/1367-2630/15/1/013008

(13) Shirane, G., Nathans, R., & Chen, C. W. (1964). Magnetic Moments and Unpaired Spin Densities in the Fe-Rh Alloys. *Physical Review, 134*(6A). doi:10.1103/physrev.134.a1547

(14) Rosenberg, M., Kuncser, V., Crisan, O., Hernando, A., Navarro, E., & Filoti, G. (1998). A Mössbauer spectroscopy and magnetic study of FeRh. *Journal of Magnetism and Magnetic Materials, 177-181*, 135-136. doi:10.1016/s0304-8853(97)00662-8

(15) Uhlíř, V., Arregi, J. A., & Fullerton, E. E. (2016). Colossal magnetic phase transition asymmetry in mesoscale FeRh stripes. *Nature Communications, 7*(1). doi:10.1038/ncomms13113

(16) Takahashi, M., & Oshima, R. (1995). Stress Induced Phase Transition of Iron-Rhodium Alloys. *Le Journal De Physique IV, 05*(C8). doi:10.1051/jp4:1995875

(17) Gruner, M. E., Hoffmann, E., & Entel, P. (2003). Instability of the rhodium magnetic moment as the origin of the metamagnetic phase transition inα−FeRh. *Physical Review B, 67*(6). doi:10.1103/physrevb.67.064415

(18) Castiella, M., Gatel, C., Bobo, J. F., Ratel-Ramond, N., Tan, R., Respaud, M., & Casanove, M. J. (2015). Structural investigation of magnetic FeRh epitaxial films. *Materials Research Express, 2*(8), 086401. doi:10.1088/2053-1591/2/8/086401

(19) Frey, H. (2015). Particle Beam Sources. *Handbook of Thin-Film Technology,*181-224. doi:10.1007/978-3-642-05430-3_8

(20) Aikoh, K., Kosugi, S., Matsui, T., & Iwase, A. (2011). Quantitative control of magnetic ordering in FeRh thin films using 30 keV Ga ion irradiation from a focused ion beam system. *Journal of Applied Physics, 109*(7). doi:10.1063/1.3549440

(21) Tohki, A., Aikoh, K., Iwase, A., Yoneda, K., Kosugi, S., Kume, K., . . . Matsui, T. (2012). Effect of high temperature annealing on ion-irradiation induced magnetization in FeRh thin films. *Journal of Applied Physics, 111*(7). doi:10.1063/1.3687133

(22) Aikoh, K., Tohki, A., Matsui, T., Iwase, A., Satoh, T., Takano, K., . . . Kinoshita, T. (2012). MFM and PEEM observation of micrometre-sized magnetic dot arrays fabricated by ion-microbeam irradiation in FeRh thin films.*Journal of Synchrotron Radiation, 19*(2), 223-226. doi:10.1107/s0909049511054057

(23) Alonzo-Medina, G. M., González-González, A., Sacedón, J. L., & Oliva, A. I. (2013). Understanding the thermal annealing process on metallic thin films. *IOP Conference Series: Materials Science and Engineering, 45*, 012013. doi:10.1088/1757-899x/45/1/012013

(24) Chen, S., Chen, S., & Kuo, P. (2009). L10 FePt thin films with high coercivity and fine grain by rapid thermal annealing with high heating ramp rate. *Thin Solid Films, 517*(17), 5176-5180. doi:10.1016/j.tsf.2009.03.178

(25) Verhoeven, J. (1992). Practical surface analysis by Auger and X-Ray photoelectron spectroscopy. *Applied Surface Science, 55*(1), 95. doi:10.1016/0169-4332(92)90384-a

(26) Russ, J. C. (1984). Energy Dispersive Spectrometers. *Fundamentals of Energy Dispersive X-ray Analysis,* 17-41. doi:10.1016/b978-0-408-11031-0.50006-7

(27) Forbest, R. (1997). Understanding how the liquid-metal ion source works. *Vacuum, 48*(1), 85-97. doi:10.1016/s0042-207x(96)00227-8

(28) Binnig, G., Quate, C. F., & Gerber, C. (1986). Atomic Force Microscope. *Physical Review Letters,56*(9), 930-933. doi:10.1103/physrevlett.56.930

(29) Rota, A., Contri, S., Gazzadi, G., Cottafava, S., Gualtieri, E., & Valeri, S. (2006). Focused ion beam induced swelling in MgO(001). *Surface Science, 600*(18), 3718-3722. doi:10.1016/j.susc.2006.01.084

(30) Unocic, K., Mills, M., & Daehn, G. (2010). Effect of gallium focused ion beam milling on preparation of aluminium thin foils. *Journal of Microscopy, 240*(3), 227-238. doi:10.1111/j.1365-2818.2010.03401.x

8 List of abbreviations

AF – Antiferromagnetic, Antiferromagnetism;

AF-FM – Antiferromagnetic to Ferromagnetic (phase transition);

AFM – Atomic Force Microscopy;

FeRh – Iron-Rhodium alloy;

FIB – Focused Ion Beam;

FM – Ferromagnetic, Ferromagnetism;

LMIS – Liquid Metal Ion Source;

MFM – Magnetic Force Microscopy;